Convective distribution of dust over the Arabian Peninsula: the impact of model resolution

Jennie Bukowski[1], Susan C. van den Heever[1]

[1] Department of Atmospheric Science, Colorado State University, Fort Collins, CO

Correspondence to: Jennie Bukowski (jennie.bukowski@colostate.edu)

Abstract

Along the coasts of the Arabian Peninsula, convective dust storms are a considerable source of mineral dust to the atmosphere. Reliable predictions of convective dust events are necessary to determine their effects on air quality, visibility, and the radiation budget. In this study, the Weather Research and Forecasting Model coupled with Chemistry (WRF-Chem) is used to simulate a 2016 summertime dust event over the Arabian Peninsula and examine the variability in dust fields and associated vertical transport due to the choice of convective parameterization and convection-allowing versus parameterized convection. Simulations are run at 45 km and 15 km grid spacing with multiple cumulus parameterizations, and are compared to a 3 km simulation that permits explicit dry and moist convective processes. Five separate cumulus parameterizations at 15 km grid spacing were tested to quantify the spread across different parameterizations. Finally, the impact these variations have on radiation, specifically aerosol heating rates is also investigated.

On average, in these simulations the convection-permitting case produces higher quantities of dust than the parameterized cases in terms of dust uplift potential, vertical dust concentrations, and vertical dust fluxes. Major drivers of this discrepancy between the simulations stem from the convection-allowing case exhibiting higher surface windspeeds during convective activity, lower dust emission wind threshold velocities due to drier soil, and more frequent, stronger vertical velocities which transport dust aloft and increase the atmospheric lifetime of these particles. For aerosol heating rates in the lowest levels, the shortwave effect prevails in the convection-permitting case with a net cooling effect, whereas a longwave net warming effect is present in the parameterized cases. The spread in dust concentrations across cumulus parameterizations at the same grid resolution (15 km) is an order of magnitude lower than the impact of moving from parameterized towards explicit convection. We conclude that tuning dust emissions in coarse resolution simulations can only improve the results to first-order and cannot fully rectify the discrepancies originating from disparities in the representation of convective dust transport.

1) Introduction

Airborne mineral dust is an important atmospheric aerosol (Zender et al., 2004; Ginoux et al., 2012): dust reduces visibility (e.g. Mahowald et al., 2007; Baddock et al., 2014; Camino et al., 2015) and is detrimental to the human respiratory system (Prospero, 1999; van Donkelaar et al., 2010; Stafoggia et al., 2016), but also plays a vital role in

32 fertilizing iron-deficient maritime ecosystems (Martin, 1991; Bishop et al., 2002; Mahowald et al., 2005; Jickells
33 and Moore, 2015). Dust particles function as cloud condensation nuclei (e.g. Lee et al., 2009; Manktelow et al.,
34 2009; Twohy et al., 2009; Karydis et al., 2011) and ice nuclei (e.g. DeMott et al., 2003; Field et al., 2006; Knopf and
35 Koop, 2006; Boose et al., 2016), thereby altering cloud development and properties. Furthermore, mineral dust is of
36 interest due to its distinctive optical properties; dust both scatters and absorbs shortwave and longwave radiation
37 (e.g. Tegen et al., 1996; Kinne et al., 2003; Dubovik et al., 2006) modifying atmospheric thermodynamics and the
38 earth's energy budget in the process (e.g. Slingo et al., 2006; Sokolik and Toon, 2006; Heald et al., 2014).

39 The influence of atmospheric mineral dust is widespread in the weather and climate system, yet generating skillful
40 forecasts of dust concentrations and their temporal and spatial evolution has been difficult to achieve. Several
41 studies suggest that including the radiative effects of mineral dust in numerical weather prediction (NWP) could
42 refine the radiation balance of these models and improve forecasts (Kischa et al., 2003; Haywood et al., 2005; Pérez
43 et al., 2006). Advances in climate models have been made by incorporating time-varying dust sources and climate-
44 dust feedbacks in the radiative forcing calculations (Kok et al., 2014; Woodage and Woodward, 2014; Kok et al.,
45 2018). However, these potential improvements are contingent upon the quality of the dust model and initialization
46 data, which models are known to be especially sensitive to. As such, substantial discrepancies exist across global
47 models of similar resolution (Huneeus et al., 2011), and across regional models (Uno et al., 2006; Todd et al., 2008)
48 in the magnitude of predicted dust flux from the surface to the atmosphere.

49 A major challenge in modeling dust processes is the scales of motion involved in its emission and subsequent
50 transport. Dust particles mobilize from the surface due to wind erosion of arid soils, a mechanism that occurs on the
51 micron scale, but once airborne mineral dust can deposit locally or be transported on the synoptic to global scales.
52 Dust events initiate from both large-scale and synoptic dynamical flow regimes, as well as mesoscale features.
53 Synoptic scale uplift phenomena include monsoon troughs (e.g. Marsham et al., 2008), Shamal winds (e.g. Yu et al.,
54 2015) and frontal systems (e.g. Beegum et al. 2018), while dynamical effects on smaller (meso) scales can raise dust
55 through the production of convective outflow boundaries, or haboobs, (e.g. Miller et al. 2008), daytime turbulence
56 or dry convective processes (e.g. Klose and Shao, 2012), and the morning mixing of nocturnal low level jet (NLLJ)
57 momentum to the surface (e.g. Fiedler et al. 2013). When considering only meteorological dust sources, wind drives
58 dust emissions, meaning that the underlying processes that contribute to the wind fields must be resolved in a model
59 to create an accurate dust forecast.

60 Current aerosol forecast and climate models are run at fine enough grid-spacing to simulate synoptic events but still
61 typically employ cumulus parameterizations, which are incapable of resolving dry and moist mesoscale updrafts and
62 downdrafts that can potentially loft and / or scavenge dust. Schepanski et al. (2015) found that online dust models
63 are likely to be most sensitive to the initialization data compared to other model options, which adds additional
64 uncertainty to dust forecasts. Pope et al. (2016) and Largeron et al. (2015) both postulated that an inadequate
65 representation of convection in coarse model simulations, specifically the underestimation of high surface
66 windspeeds in mesoscale haboobs, is a major contributor to errors in dust models.

67

68 The misrepresentation of dust concentrations in models with cumulus parameterizations has been investigated across

69 several modeling platforms, mostly from the perspective of dust lofting mechanisms at the surface. Heinold et al.

70 (2013) ran the UK Met Office Unified Model (UM) over West Africa with offline dust emissions, and found that of

71 the factors they tested, the model was most sensitive to explicit versus parameterized convection. Furthermore, in

72 the Heinhold et al. (2013) study, dust emissions were reduced as grid resolution was increased to convection-

73 permitting scales by roughly 50%. This was found to be due to the parameterized simulations underestimating moist

74 convective activity but drastically overestimating the NLLJ dust uplift mechanism, a similar relationship to that

75 originally identified in Marsham et al. (2011).

76 Conversely, studies using different numerical dust models have identified other relationships between horizontal

77 resolution and dust emissions. Roberts et al. 2018 also used UM to investigate this relationship over the Sahara and

78 Sahel and reported little change in the dust emissions when moving from parameterized to explicit convection, but

79 also noted that the NLLJ maximum decreased as the convective maximum increased. Reinfried et al. (2009)

80 simulated a haboob case study from Morocco with the Lokal Modell - MultiScale chemistry aerosol transport (LM-

81 MUSCAT, since renamed COSMO-MUSCAT) regional model and found increased dust emissions in a convection-

82 allowing simulation versus those with cumulus parameterizations. They also established that the model was more

83 sensitive to the choice of cumulus parameterization rather than the change in horizontal resolution. Similarly, Bouet

84 et al. (2012) identified an increase in dust emissions with increasing model resolution using the Regional

85 Atmospheric Modeling System coupled to the Dust Prediction Model (RAMS-DPM) while simulating a Bodélé

86 depression case study. Ridley et al. (2013) showed that global aerosol models with parameterized convection were

87 also sensitive to model resolution and that higher horizontal resolution led to higher dust emissions.

88

89 With the added computational expense of running aerosol code, the resolution of dust forecast models lags relative

90 to their weather-only prediction counterparts for both global and regional prediction systems (Benedetti et al., 2014;

91 Benedetti et al., 2018). Global dust forecasts generated by several aerosol models are available through the Sand and

92 Dust Storm Warning Advisory and Assessment System (SDS-WAS) (http://www.wmo.int/sdswas), but none

93 of the models in the SDS-WAS are currently run at fine enough grid-spacing to be considered convection-permitting

94 (SDS-WAS Model inter-comparison and forecast evaluation technical manual; last updated January, 2018). While

95 regional numerical weather prediction models have moved into convection-permitting scales, the added

96 computational cost of aerosol parameterizations means that convective parameterizations will be a necessity for

97 longer in models that employ online aerosol predictions. It is also clear that horizontal model resolution remains an

98 understudied factor in regional dust modeling. As such, exploring differences across cumulus parameterizations and

99 those relative to convection-permitting resolutions continues to be relevant and vital to better understand aerosol

100 forecasting and aerosol-cloud-environment interactions.

101 While previous studies have begun to examine the effect of horizontal model resolution on dust emissions and

102 airborne dust concentrations, there are several factors that warrant more investigation. As it stands, there is little

103   agreement on the sign of the response in dust emissions to a change in horizontal model resolution, which seems to

104   vary based on the regional model being utilized. Most studies have concentrated on the change in dust emissions

105   based on moving from parameterized convection to convection-allowing scales, while ignoring the possible

106   sensitivity due to the choice of the cumulus parameterization itself. Furthermore, much of the previous literature

107   focused on how the increase in resolution affects convective outflow boundaries and surface / near-surface processes

108   as dust sources, rather than convective transport and the vertical redistribution of dust and its radiative effects at

109   different levels of the atmosphere. In this paper, we seek to address these limitations in the understanding of the

110   effects of horizontal model resolution on dust concentrations. The goal of the research presented here is therefore to

111   quantify the sign and magnitude in the response of modeled dust fields in a regional numerical model to increasing

112   horizontal resolution.

113   In order to achieve our stated goal, we will use numerical simulations of a case study to examine the variability in

114   dust emissions and vertical dust concentrations and fluxes due to (1) the choice of convective parameterization, (2)

115   convection-allowing versus parameterized convection, and (3) the impact of these variations on radiation,

116   specifically aerosol heating rates. These simulations are performed using the Weather Research and Forecasting

117   Model coupled with Atmospheric Chemistry (WRF-Chem) (Skamarock et al., 2008; Grell et al., 2005; Fast et al.,

118   2006) a platform that has been tested for its sensitivity to vertical resolution for dust extinction coefficient profiles

119   (Teixeira et al., 2015) and horizontal model resolution and convective transport for chemical species such as carbon

120   monoxide (e.g. Klich and Fuelberg, 2013), but not for dust. These simulations will represent a case study of a

121   summertime coastal convective dust event over the Arabian Peninsula, a relatively understudied region compared to

122   areas such as the Sahara (Jish Prakash et al., 2015), despite being the world's second largest dust emission region

123   (Tanaka and Chiba, 2004).

124   This paper is part of a larger body of collaborative work conducted by the Holistic Analysis of Aerosols in Littoral

125   Environments (HAALE) research team under the Office of Naval Research Multidisciplinary Research Program of

126   the University Research Initiative (MURI). The primary goal of the HAALE-MURI project is to isolate the

127   fundamental environmental factors that govern the spatial distribution and optical properties of littoral zone aerosols.

128   The study discussed in this manuscript focuses on advancing our understanding in the role that convection plays in

129   the redistribution of dust aerosol and its radiative effects along the coast of arid regions, and seeks to quantify the

130   uncertainty in forecasted dust distributions stemming from the representation of convective processes in a regional

131   model.

132   The manuscript is organized as follows: an overview of the WRF-Chem model and physics setup (Sect. 2.1), dust

133   model setup (Sect. 2.2), information about the cumulus parameterizations and model resolution (Sect. 2.3), and

134   analysis methods in Sect. 2.4. A description of the case study is found in Sect. 2.5. The results are outlined in Sect.

135   3, with a discussion on the temporal evolution of dust concentrations and dust uplift potential in Sect. 3.1, vertical

136   distributions and fluxes of dust in Sect. 3.2, and the effect on aerosol radiative heating rates in Sect. 3.3. A

137   discussion of the results and implications for the community are located in Sect. 4 and a summary of the findings of
138   this study are reviewed in Sect. 5.

139   **2) Case study and model description**

140   **2.1) WRF-Chem model description and physics**

141   To investigate the Arabian Peninsula case study, WRF-Chem version 3.9.1.1 was used to simulate the dust outbreak

142   meteorology and aerosol fields. WRF-Chem is an online numerical chemical transport model that allows for

143   interactive aerosol processes, including feedbacks between the meteorology, aerosol, and radiation. The model was

144   coupled to the Goddard Chemistry Aerosol Radiation and Transport (GOCART) module (Ginoux et al., 2001),

145   which allowed for feedbacks between the meteorology and aerosols and is described in more detail in Sect. 2.2. The

146   model was tested with and without dust initial and boundary conditions from the Community Atmosphere Model

147   with Chemistry (CAM-Chem) global model (Emmons et al. 2010). The concentrations of dust advected through the

148   lateral boundary conditions was too small to have an effect on the results, and the initial conditions introduced a

149   spurious decreasing integrated dust trend over time when modeled aerosol optical depth (AOD) was compared to

150   AERONET observations. While the initial conditions led to a higher integrated dust mass, it did not change the

151   conclusions of the study. To remove this factor and focus more on the meteorological processes that actively loft and

152   transport dust in real-time, no chemistry or aerosol initial / lateral boundary conditions were used. Rather, the

153   aerosol fields were initialized with zero concentrations and were allowed to evolve naturally from the model

154   meteorology, aerosol, surface and radiation processes.

155

156   The meteorological and sea surface temperature initial and lateral boundary conditions were sourced from the 0.25

157   degree, 6-hourly Global Data Assimilation System Final Analysis (GDAS-FNL). The model was run from 00:00:00

158   UTC on 02-Aug-2016 to 00:00:00 UTC on 05-Aug-2016 producing output at 30-minute intervals. The following

159   model parameterizations were employed and kept constant across the simulations, with similar WRF physics options

160   being utilized elsewhere to study dust effects (e.g. Alizadeh Choobari et al. 2013): Morrison double-moment

161   microphysics (Morrison et al., 2005; 2009), RRTMG longwave scheme (Iacano et al., 2008), Goddard shortwave

162   radiation scheme (Chou and Suarez, 1999), the Noah Land Surface Model with multiparameterization options (Niu

163   et al., 2011; Yang et al., 2011), and the MYNN level 3 boundary layer parameterization (Nakanishi and Niino, 2006;

164   2009). The convective parameterizations and horizontal resolutions tested will be discussed in Sect. 2.4. A summary

165   of the physics options utilized can be found in Table 1.

166

167   **2.2) GOCART dust emissions and dust uplift potential**

168   WRF-Chem is coupled to the GOCART dust module, which parameterizes the emission of dry mineral dust mass

169   from the surface. GOCART is single-moment in mass, meaning there is no number information available to change

170   the number of cloud condensation nuclei or ice nuclei in the microphysics. As such, the indirect effects of dust

171   cannot be simulated with this setup. Through this model, dust is emitted to the atmosphere in 5 discrete effective

172   radii bins [0.5, 1.4, 2.4, 4.5, and 8.0 μm] based on Eq. (1):

173    $F_p = CSs_p\,U^2(U - U_t)\ if\ U > U_t$ (1)

174   In Eq. (1), F_p is the dust flux from the surface [kg m^{-2} s^{-1}] for each of the radii bins (p), S represents the wind erosion

175   scaling factor [0 to 1] established by the Ginoux et al. (2004) soil erodibility map, s_p is the fraction of each size class

176   within the soil [0 to 1] based on the silt and clay fraction of the soil type, U is the 10 m wind speed [m s^{-1}], and U_t is

177   the threshold velocity of wind erosion [m s^{-1}]. C is a tuning constant (set here to a default 1 kg s^2 m^{-5}), which can be

178   set by the user to increase or decrease the total dust flux based on regional observations (e.g. Zhao et al., 2010;

179   Kalenderski et al., 2013; Dipu et al., 2013). If the wind speed is less than the threshold velocity, no dust will loft

180   from the surface. Most of the terms in Eq. (1) are time invariant (C,S,s_p), except for the wind speed (U) and wind

181   erosion threshold (U_t). U_t is a function of soil wetness, and is calculated with the relationship found in Eq. (2):

182    $U_t = \begin{cases} 6.5\sqrt{\dfrac{\rho_p - \rho_a}{\rho_a} gD_p}\,(1.2 + log_{10}w_{soil}) & if\ w_{soil} < 0.5 \\ \infty & if\ w_{soil} \geq 0.5 \end{cases}$ (2)

183   For Eq. (2), ρ_p is the dust particle density [kg m^{-3}], ρ_a is the density of air [kg m^{-3}], g is gravitational acceleration [m

184   s^{-2}], and w_{soil} is the soil wetness fraction [0 to 1]. Similar to Eq. (1), Eq. (2) includes a threshold, whereby above a

185   soil wetness of 0.5, no dust will be emitted. If the threshold criteria are met and dust lofts from the surface, it is then

186   transported based on the simulated meteorological fields from WRF, including advection, convection, and turbulent

187   mixing, and is removed from the atmosphere via gravitational settling and wet deposition. Here, wet deposition is

188   included as a scavenging mechanism to provide a more realistic picture of the moist convection transport process.

189   Aerosol radiation interactions in the shortwave and longwave (Barnard et al., 2010) are included in the simulations

190   to understand the implications that lofted dust has on the energy budget of the case study and are discussed in Sect.

191   3.3.

192   Before dust can amass in and influence the atmosphere, it must first be emitted from the surface. Because of the

193   threshold values included in the GOCART dust parameterization equations (Eq. 1-2), it is important to understand

194   how often the modeled near-surface wind speeds exceed the wind threshold value. A parameter useful in describing

195   the influence of the wind on dust emissions is Dust Uplift Potential (DUP), proposed by Marsham et al. (2011) and

196   based on Marticorena and Bergametti (1995). The DUP parameter is an offline approximation for the relative

197   amount of dust expected to loft from the surface. DUP is a convenient way to perform first order sensitivity tests on

198   the meteorology without having to re-run the model, and provides a framework for deconvolving the variables in Eq.

199   (1-2). Here, we have adapted the DUP parameter from Marsham et al. (2011) (Eq. 4) into three variations (Eq. 3-5),

200   which allows researchers to vary the complexity of the analysis by including more, or fewer degrees of freedom.

201    $DUP(U) = U^3\left(1 + \dfrac{A}{U}\right)\left(1 - \dfrac{A^2}{U^2}\right)$ (3)

202    $DUP(U, U_t) = U^3\left(1 + \dfrac{U_t}{U}\right)\left(1 - \dfrac{U_t^2}{U^2}\right)$ (4)

203 $$DUP(U, U_t, S) = SU^3 \left(1 + \frac{U_t}{U}\right)\left(1 - \frac{U_t^2}{U^2}\right) \tag{5}$$

204 In Eq. (3), U_t is set to a constant wind speed, *A,* thereby making DUP a function of only the near-surface wind

205 speed; for the purpose of this paper U_t is set to 5 m s^{-1}, but has been tested elsewhere across the range of 5-10 m s^{-1}

206 (e.g. Marsham et al., 2011; Cowie et al., 2015; Pantillon et al., 2015). This simplified equation for dust uplift has

207 been used in previous dust studies, and is useful to include here to place this manuscript in the context of existing

208 literature. Eq. (4) is slightly more intricate in that it considers the model evolution of U_t due to changing soil wetness

209 from precipitation and land-surface processes, calculated by Eq. (2). Lastly, Eq. (5) builds on Eq. (4) by including

210 the soil erodibility scaling factor (*S*), which recognizes that the *U* and U_t relationship is valid only if it occurs over

211 potential dust source regions. Since *U*, U_t, and S are entangled in the GOCART dust parametrization found in Eq.

212 (1-2), the seemingly minor variations between the DUP parameters in Eq. (3-5) are crucial for isolating which

213 processes, or combination of processes, are sensitive to the horizontal resolution of the model, and hence to the

214 analysis performed here.

215 **2.3) Domain, nesting, and cumulus parameterizations**

216 Several horizontal model grid-spacings (45 km, 15 km, and 3 km) of the Arabian Peninsula domain (Fig. 3) were

217 tested to identify the sensitivity of modeled dust concentrations to the model's horizontal resolution. For the two

218 coarsest simulations (45 km and 15 km), cumulus parameterizations were employed to represent shallow and deep

219 convection. The 45 km simulation was run with only the Betts–Miller–Janjic (BMJ) cumulus parameterization

220 (Janjic, 1994), while five different cumulus parameterizations were tested for the 15 km simulations, including the

221 BMJ, Kain–Fritsch (KF) (Kain, 2004), Grell 3D Ensemble (GD) (Grell, 1993; Grell et al., 2002), Tiedtke (TD)

222 (Tiedtke, 1989; Zhang et al., 2011), and Simplified Arakawa–Schubert (AS) (Arakawa and Schubert, 1974; Han and

223 Pan, 2011) schemes, which will determine the sensitivity of dust lofting to different cumulus parameterizations. A

224 15 km simulation with no cumulus parameterization was also run, but the results were similar and within the spread

225 of the 15 km simulations that employed cumulus parameterizations and are not included here. The finest resolution

226 simulation (3 km) was run at convection-permitting scales and hence no cumulus parameterizations were invoked.

227 The 3 km simulation was initialized as a one-way nest from the 15 km BMJ simulation, which served as its parent

228 lateral boundary conditions. Other combinations of nests were tested, but the results were not sensitive to which 15

229 km simulation was used as the parent nest, or lateral boundary conditions, for the 3 km simulation. A summary of

230 the model domains is also found in Fig. 3.

231 The cumulus parameterizations tested in this study for the 15 km simulations vary in their methods for triggering

232 and then characterizing convective processes at the sub-grid scale level. BMJ is a moisture and temperature

233 adjustment scheme that acts to restore the pre-convective unstable thermodynamic profile to a post-convective stable

234 and well-mixed reference profile, while the other cumulus parameterizations (KF, GD, TD, AS) employ a mass-flux

235 approach to determine updraft and downdraft mass transport. Across the mass-flux parameterizations, GD is unique

236 in that it computes an ensemble of varying convective triggers and closure assumptions and then feeds the ensemble

237 mean back to the model. Furthermore, all five schemes represent shallow convection in addition to deep convection,

238 the mass-flux schemes include detrainment of water and ice at cloud top, and AS and TD are formulated to include

239 momentum transport in their calculations. These differences across parameterizations will result in varying updraft

240 and downdraft speeds and precipitation rates, which will have consequences for the vertical transport of airborne

241 dust, as well as the strength of convective outflow boundaries and therefore dust emission at the surface. Several

242 cumulus parameterization schemes were tested to introduce spread into the solutions and to represent the 15 km

243 results as a 5-member ensemble mean with uncertainty estimates. Because this paper seeks to investigate the effect

244 of horizontal resolution on dust transport, comparing individual cumulus schemes against one another is outside the

245 scope of this study.

2.4) Averaging and analysis methods

247 Because the representation of convective processes varies across the simulations, the results will focus on composite

248 statistics from the three-day case study. The authors make no attempt to track and match individual convective

249 elements across simulations, as their triggering, timing, and development (or lack of development) will fluctuate

250 depending on the model resolution and cumulus parameterization, thus making a truly consistent analysis

251 problematic. Instead, this paper takes a step backward and aims to quantify in an average sense, how the choice of

252 horizontal resolution and parameterized convection affects dust concentrations in the WRF-Chem model across the

253 Arabian Peninsula. The analyses and averages are processed within the yellow box shown in Fig. 3, disregarding all

254 other grid points outside the Arabian Peninsula study area. Analyses that are averaged in time are only averaged

255 over the last two days of the simulation (00:00:00 UTC on 03-Aug-2016 to 00:00:00 UTC on 05-Aug-2016) to

256 account for model spin up in the first 24 hours. All results are summed over the five dust bins in the GOCART

257 model rather than being treated separately. Lastly, the results from the five 15 km simulations are averaged together

258 to produce a mean 15 km resolution response, and is presented, along with the maximum and minimum spread

259 across these simulations for reference.

2.5) Case study overview

261 The dust event simulated for this study occurred during August 2-5, 2016 across the Arabian Peninsula, originating

262 from a combination of synoptic and mesoscale dust sources. A meteorological analysis of this event, including an

263 attribution of specific dust sources to meteorological features can be found in Miller et al. (2019) and will not be

264 reiterated in detail here. Rather, a snapshot of the meteorology and dust fields from the WRF-Chem simulation on

265 August 3rd at 15:00:00 UTC can be found in Fig. 1-2 as a reference to the typical meteorological setup for this case

266 study.

267 For this event, the high summertime temperatures in the desert of the Arabian Peninsula produce a thermal low

268 couplet at the surface, with one low centered over Iraq and the other over the Rub' al Khali desert in Saudi Arabia

269 (Fig. 1.c). The local low-pressure couplet leads to cyclonic surface winds between these two areas (Fig. 1.e),

270 comprised of northerly flow from Iraq into Saudi Arabia, with retuning southerly flow from Oman over the Persian

271 Gulf and into Kuwait, and is a major non-convective contributor to the dust budget for this case study (Fig. 1.f). In

272 addition to these large-scale flow patterns, a daytime sea breeze brings moist, maritime air from the coast of Yemen

273 and Oman inland into the otherwise arid Saudi Arabian basin (Fig. 1.e and 1.d). This moisture gradient is also

274 evident in the skew-t diagrams, which represent an inland radiosonde release site at Riyadh (Fig. 2.a), and a site

275 closer to the coast in Abha (Fig. 2.b), both located in Saudi Arabia. There is a stark difference in low-level moisture

276 between the two sites, although both display a subsidence inversion aloft between 500 and 600 hPa. Furthermore,

277 nocturnal low-level jets form along the Zagros mountains in Iran and Iraq, and the Red sea, both of which have been

278 studied previously in the literature (Giannakopoulou and Toumi, 2011; Kalenderski and Stenchikov, 2016).

279 Due to the region's inherent moisture constraints, convection is limited spatially to the coastal regions of the

280 Arabian Peninsula, as is most summertime convective and non-convective precipitation in this region (e.g. Shwehdi,

281 2005; Almazroui, 2011; Hasanean and Almazroui, 2015; Babu et al., 2016). Moist convective cells develop along a

282 low-level convergence line between the northerly basin flow and sea breeze front (Fig. 1.g and 1.h) aided by

283 elevated terrain in Yemen and Oman (Fig. 1.a). This convective setup along the southern portion of the Arabian

284 Peninsula is a feature evident in each day of this case study, initializing diurnally in the local late afternoon and early

285 evening, and thereby providing three days of data for analysis, with the height of convective activity occurring on

286 August 3rd. Individual convective cells form along the convergence line, a typical Middle Eastern characteristic

287 (Dayan et al., 2001), but do not organize further, owing to a lack of upper-level synoptic support and insufficient

288 moisture in the interior of the peninsula. Nevertheless, the convective line does produce outflow boundaries, which

289 loft dust from the surface and are the main convective dust source for this case study. More information on model

290 validation of this study, including comparisons of these simulations with AOD observations can be found in Saleeby

291 et al. (2019), which shows that WRF-Chem systematically underestimates dust AOD for this event.

292 **3) Results**

293 **3.1) Temporal evolution**

294 **3.1.1) Dust uplift potential**

295 The first process of interest in determining the sensitivity of modeled dust concentrations to horizontal resolution in

296 WRF-Chem is the amount of dust lofted from the surface to the atmosphere. Fig. 4 depicts the average DUP for the

297 simulations at each 30-minute output, using Eq. (3-5) to separate out the importance of the different mechanisms

298 regulating dust emissions.

299 Regardless of which DUP parameter is used, almost all of the simulations capture the bimodal daily maximum in

300 dust emissions in the local mid-morning (6 UTC) and late afternoon (13 UTC) due to the mixing of the NLLJ to the

301 surface and convective outflow boundaries, respectively. The only resolution where the bimodality is absent is the

302 45 km simulation, which captures the NLLJ mechanism, but misses the second convective activity maximum. The

303 coarsest simulation overestimates the near-surface wind speeds related to the NLLJ mechanism, which subsequently

304 inhibits convection later in the day. Because of this, the 45 km simulation has the highest DUP(U) (Fig. 4.a) based

305   only on wind speed (Eq. 3), a result similar to the Heinhold et al. (2013) and Marsham et al. (2011) studies over the

306   Sahara.

307   However, when taking the calculated threshold wind velocity into account (Eq. 4), the convection-allowing

308   simulation (3 km) displays the strongest $DUP(U,U_t)$ at the local late afternoon convective maximum (Fig. 4.c). For

309   this to be the case compared to the $DUP(U)$ parameter, the 3 km simulation must have a lower threshold wind

310   velocity (Fig. 5.a) than the simulations with parameterized convection. Since the threshold wind velocity is

311   proportional to soil wetness (Eq. 2), this implies that the convection-permitting simulation will on average have drier

312   soil, or more grid points below the soil wetness threshold than the parameterized simulations. Rainfall is generated

313   differently in parameterized versus convection-allowing simulations, and it has been well documented that

314   parameterized simulations produce more widespread light rainfall, whereas more intense rainfall tends to develop

315   over smaller areas in convection-allowing simulations (e.g. Sun et al., 2006; Stephens et al., 2010). From a domain

316   average perspective, rainfall in the 3 km simulation will cover less area, leading to the soil moisture threshold not

317   being exceeded as frequently compared to the parameterized cases.

318   This spatial difference in rainfall leads to the 3 km case having drier soil on average across the domain, which is

319   evident in the surface fluxes represented by the Bowen ratio of sensible to latent heat fluxes in Fig. 5.c. When the

320   Bowen ratio is above one, more of the surface heat exchange with the atmosphere is in the form of sensible heat

321   flux, rather than latent heat flux. Dry soils are characterized by low values of latent heat flux, and therefore exhibit

322   higher Bowen ratios. The 3 km simulation exhibits a higher Bowen ratio on August 3rd and 4th, indicating that the

323   soil is on average drier in the convection-permitting simulation. This result implies that disparities in land surface

324   properties across the varying model grid resolutions are important for modulating dust emissions, both from the

325   perspective of convection-allowing versus parameterized convection and associated precipitation, as well as latent

326   and sensible heat fluxes.

327   Adding on to the complexity of the DUP parameter, when the location of dust sources is considered in the

328     $DUP(U,U_t,S)$ calculations (Eq. 5), some of variability between the local NLLJ and convection maxima is lost in the

329   3 km simulation (Fig. 4.e) on August 3rd. Also, including the scaling factor reduces the magnitude of the DUP

330   parameter to roughly 10% of the initial values for $DUP(U)$ and $DUP(U,U_t)$. Incorporating the dust source function in

331   DUP works not only as a scaling factor for the magnitude of potential dust emissions, but also impacts the relative

332   importance of dust production mechanisms (NLLJ versus convection). This shift is a consequence of the location in

333   which these processes occur. For instance, the reduction in the 3 km convective maximum on August 3rd between

334     $DUP(U,U_t)$ and $DUP(U,U_t S)$ signifies that convection is occurring in locations that are not active dust source

335   regions. Without information on the dust source regions, this process would be assigned an unrealistic dominance

336   over the NLLJ mechanism in terms of DUP.

337   All simulations are similar for the first 24 spin-up hours until the processes begin to diverge on August 3rd, where

338   the convection-allowing simulation produces the maximum $DUP(U,U_t,S)$ both during the local daytime and

339   nighttime hours. On the final day of the case study (August 4th), the convection-allowing simulation has the lowest

340   DUP(U,U_t,S), with the NLLJ maximum dominating over the convective maximum in both the 3 km and the 15 km

341   mean, due to reduced convective activity in the fine resolution simulations. Examining the percent difference in

342   DUP between the coarse and fine simulations (Fig. 4.b,d,f), the average percent difference between the 3 km and 15

343   km simulations is at a minimum when only wind speed is considered, and increases as the degrees of freedom in

344   DUP increases. For the DUP(U,U_t,S) case, the average percent difference is between 10-65% lower in the 15 km

345   simulations than the convection-permitting simulation, with a maximum difference of 85% and a spread across

346   parameterizations of 20%. This implies that the convection-allowing WRF-Chem simulation has the potential to loft

347   up to 85% more dust than those with parameterized convection.

348   **3.1.2) Vertically integrated dust mass**

349   The differences in DUP(U,U_t,S), or dust flux from the surface to the atmosphere, specifically the enhanced values

350   for the convection-permitting simulation on August 3rd, will lead to more dust lofting than in the coarse simulations.

351   To see how differences in the dust emissions translate into differences in airborne concentrations of dust, Fig. 6

352   demonstrates the temporal evolution of the spatially averaged, vertically integrated dust mass throughout the vertical

353   column. Here, the convection-allowing simulation records upwards of 150% more integrated dust mass compared to

354   the coarse resolution simulations. Across the coarse simulations, the 45 km and 15 km runs have similar vertically

355   integrated dust magnitudes, despite the temporal differences in DUP(U,U_t,S). This is due to the overestimation of

356   the NLLJ in the 45 km simulations being offset by the enhanced convective dust lofting in the 15 km simulations.

357   The discrepancy in the diurnal maxima across horizontal resolutions is similar to the results of the UM in Marsham

358   et al. (2011) and Heinhold et al. (2013). Yet, the results here differ in that both of these previous studies found a

359   stronger NLLJ response in 12 km simulations with convective parameterizations than was found here in the 15 km

360   parameterized ensemble. In contrast to the findings of Marsham et al. (2011) and Heinhold et al. (2013), dust

361   emissions and airborne dust mass increases in the WRF-Chem simulations in the convection-allowing simulation,

362   which is in closer agreement to the studies of Reinfried et al. (2009) and Bouet et al. (2012) who used COSMO-

363   MUSCAT and RAMS-DPM respectively. Considering each study used a different model and therefore physics, it is

364   unsurprising that the results vary. However, it is not apparent how much of a role the region or specific case study

365   plays in this difference and is an area for future work.

366   The temporal trends in vertically integrated dust mass lag behind those observed in the DUP plots in Fig. 4.

367   Particularly at timesteps where DUP decreases, the change in integrated dust mass follows several hours later. The

368   time series of gravitational settling rates at the surface (Fig. 5.b) also lags behind the DUP trends, which implies that

369   the removal mechanisms for dust take time to act on the airborne particles once they are emitted. The rates of

370   gravitational settling are higher in the convection-permitting simulation compared to the coarse simulations because

371   more dust is available aloft to settle out. Nevertheless, Fig. 6.a suggests that this increase in gravitational settling

372   rates in the 3 km case is not enough to offset the higher dust emissions, or the vertically integrated dust quantities

373   would be similar across all the simulations. The fact that the vertically integrated dust values are higher in the 3 km

374   simulation, despite higher rates of gravitational settling, implies there must be a mechanism that acts to keep dust

375 suspended longer in the convection-permitting simulations than in those with parameterized convection. There are

376 clearly more processes occurring above the surface to influence the vertically integrated dust quantities than just a

377 simple surface emission to surface deposition ratio. This will be further deconstructed by examining vertical profiles

378 in the following section.

379 **3.2) Vertical characteristics**

380 **3.2.1) Vertical dust and velocity profiles**

381 Moving away from vertically integrated quantities to a time and domain averaged vertical snapshot of dust (Fig.

382 7.a), the vertical dust profile follows a generally exponentially decreasing function and tapers off to low dust

383 concentrations in the range of 5-6 km above ground level (AGL). A widespread subsidence inversion is present near

384 6 km throughout the case study time period over the inner basin of the Arabian Peninsula (Fig 2), acting as a cap on

385 vertical motions and dust transport. Because dust concentrations do not vary much above this height, the plots in

386 Fig. 7 have been truncated at 9 km. There is a higher concentration of dust at every level in the convection-allowing

387 simulation compared to that in the coarse simulations. Examining the percent difference plot between the

388 convection-permitting and other simulations in Fig. 7.b, there is a difference of approximately 80% at the surface,

389 which increases upwards to ~180% at 6 km. Above this level, the percent difference between the convection-

390 permitting and coarse simulations changes sign, but the overall concentration is extremely low, and as such, the

391 authors make no attempt to assign meaning to the differences above 6 km.

392 For dust to reach higher levels in the atmosphere, it must have undergone vertical transport to move it aloft from its

393 initial source region at the surface. Several mechanisms could be responsible for vertical dust transport in the

394 Arabian Peninsula, including flow over terrain, daytime mixing (dry convection), and lastly, moist convective

395 updrafts, whose representation (explicit versus parameterized) is a defining difference between the horizontal

396 resolutions tested in this paper. Investigating the effect that increasing resolution has on updraft and downdraft

397 strength can be found in Fig. 8, which represents the mean of all vertical velocities above or below 0 m s^{-1}, including

398 points that are not vertically continuous. As resolution increases, the average range in vertical velocity also

399 increases. The simulations with parametrized convection have lower mean updraft / downdraft speeds than the

400 convection-allowing simulation, on the order ~75% weaker near the surface for the 15 km runs and ~110% weaker

401 for the 45 km run. It is known that in numerical models, the updraft radius scales with the grid spacing (e.g. Bryan

402 and Morrison, 2012), with a compensating increase in updraft speed as the radius decreases. This relationship skews

403 the frequency of vertical velocities to higher values. Irrespective of resolution, the mean updraft speeds in the WRF-

404 Chem simulations are slightly higher than the downdraft speeds, while at the surface mean downdraft speeds are

405 higher than updraft speeds, a consideration that will be discussed further in Sect. 3.2.2.

406 **3.2.2) Vertical dust flux**

407 The implication for dust transport based on vertical velocities is convoluted, since updrafts and downdrafts work

408 concurrently to redistribute aerosol. As noted in Jung et al. (2005), convective updrafts will lift aerosol particles

409 upward into the free atmosphere, while downdrafts simultaneously limit the maximum vertical extent of these

410 particles. However, the convective transport simulations in Jung et al. (2005) demonstrate that these opposing

411 processes do not act as equal opposites in time, magnitude, and space. This canon holds true for the Arabian

412 Peninsula simulations as well. Fig. 9 contains Contoured Frequency by Altitude Diagrams (CFADs) of vertical

413 velocity (Yuter and Houze, 1995) normalized by the total number of grid points in each simulation. The

414 normalization is performed to remove an artificial larger frequency in the higher resolution simulations that arises

415 because there are more grid spaces available to count. Because no vertical velocity threshold is imposed, a majority

416 of points straddle zero. To highlight variability away from the zero line, the CFAD contours are plotted on a log

417 scale.

418 Similar to the mean plots in Fig. 8, as resolution increases, so does the variability in updraft and downdraft speeds.

419 There is a striking difference between the spread in vertical velocities at all altitudes across the 45 km, 15 km mean,

420 and 3 km simulations in Fig. 9. In the 45 km run, most of the velocities straddle +/- 1-2 m s^{-1}, whereas the

421 convection-permitting simulation ranges from -10 to 30 m s^{-1}. Not only is the range larger, but the normalized

422 frequency is greater in the fine resolution simulation as well. The inference here is that stronger updrafts will

423 transport dust higher in the atmosphere, and that stronger updrafts are observed more frequently in the convection-

424 allowing simulation, thereby enhancing the vertical dust transport.

425 Combining the information on the vertical distribution of dust and updraft / downdraft speeds, it is possible to

426 calculate a domain averaged dust flux profile (Fig. 8). Again, the magnitude of the dust flux upwards and

427 downwards from the surface through 6 km AGL is higher in the convection-allowing simulation compared to the

428 parametrized simulations. Moreover, the mean near-surface upwards dust flux is stronger than that for the downward

429 dust flux, which coincides with the mean updraft speeds being slightly higher than the mean downdraft speeds at

430 these same vertical levels (Fig. 8). This relationship also holds in the dust flux CFADs (Fig. 9), in which the upward

431 and downward flux of dust has more variability in the 3 km simulation, and stronger vertical dust fluxes are more

432 frequent.

433 Similarly, there is more dust transport evident at higher vertical levels in the convection-permitting simulation,

434 which has implications for the residence time of the dust particles. As dust is transported higher in the atmosphere,

435 absent any sort of external motion or coagulation outside of gravitational settling, the atmospheric lifetime of the

436 particles will increase. Figure 10 shows the theoretical terminal velocity of dust particles in WRF-Chem using the

437 Stokes settling velocity with slip correction for pressure dependence (Fig. 10.a) and their lifetime based on different

438 starting heights in the atmosphere (Fig. 10.b), which increases exponentially away from the surface. As such, dust in

439 the convection-permitting simulation will take longer to settle out, leading to the higher observed vertically

440 integrated dust values (Fig. 5) compared to the parameterized simulations. Looking at the distribution of downdrafts

441 in the vertical velocity CFADs (Fig. 9), there is a clear bimodal signal aloft in both the convection-permitting and 15

442 km simulations, being representative of two distinct subsidence layers, which act as a cap on vertical transport. The

443 local minimum occurs around 6 km, which could explain why dust fluxes also taper off at this level.

444   At the surface, higher dust flux values are found in association with the downdrafts, producing a pronounced

445   skewness towards high, yet infrequent values of strong negative dust flux towards the ground (Fig. 9). It is

446   hypothesized that this skewness is a consequence of the dissimilar background dust conditions in the vicinity of

447   near-surface downdrafts and updrafts, similar to the results found in Siegel and van den Heever (2012), which

448   studied the ingestion of dust by a supercell storm. Updrafts originate in relatively clear air, and will consume

449   background dust and transport it upwards. However, downdrafts occur through the cold pool, and hence their source

450   is, at least partially, within the dusty cold pool. As such, downdrafts will have access to more dust and thus transport

451   more of it in the downward direction. This skewness warrants further research, preferably from an idealized

452   perspective, to better understand the relationship between storm dynamics, dust emissions, and transport.

453   In all, the increased vertical dust concentration profile and vertically integrated dust values in the 3 km run are a

454   product of several processes working together. Compared to the simulations with parameterized convection, the 3

455   km run has enhanced potential for dust uplift due to stronger resolved downdrafts and lower wind velocity

456   thresholds, higher vertical transport due to more frequent, stronger updrafts, and a lengthier theoretical residence

457   time once being lofted to higher levels.

458   **3.3) Impacts on radiation**

459   Beyond the first-order sensitivity of model resolution to dust emissions and concentrations for the Arabian Peninsula

460   case study, there are higher-order effects that disseminate from changing dust concentrations. One example being

461   the modification of atmospheric heating / cooling rates and the radiation budget due to dust absorption and scattering

462   (see Sect. 1). The domain and time averaged shortwave (SW), longwave (LW), and net dust heating / cooling rates

463   are found in Fig. 11. The average dust heating and cooling rates were calculated over the last 48 hours of the

464   simulation as a difference between the radiation tendency with dust aerosols and without. Ostensibly, since dust

465   concentrations increase in the model as resolution increases, so does the magnitude of the radiative effects. There is

466   a stronger SW cooling and LW heating effect in the 3 km simulation, and this trend follows the vertical distribution

467   of dust from Fig. 7, again tapering off near 5-6 km AGL.

468   Most interestingly, however, is the difference in the net aerosol heating rate. In the lowest layer (<1.5 km), there is a

469   sign change between the fine and coarse simulations. The SW effect in the convection-allowing simulation is strong

470   enough to elicit a net cooling effect in this near-surface layer. Conversely, the LW aerosol heating effect dominates

471   in the coarse simulations, resulting in a net warming effect. The model has a stronger shortwave effect for dust based

472   on the prescribed index of refraction, but is also related to the timing of dust emissions, considering the SW effect is

473   only active during the daytime. The difference between warming and cooling can have cascading effects on the

474   thermodynamic profile, static stability, and future convective development, which in turn impacts the relative

475   importance between convection and the NLLJ discussed earlier. The sensitivity of dust concentrations to horizontal

476   model resolution is important to understand in its own right, but furthermore, this sensitivity leads to higher-order

477   changes in model predictions. If NWP models or GCMs are going to incorporate dust radiative effects,

478 concentrations need to be highly constrained, not only to accurately capture the magnitude, but the sign of the

479 response as well.

480 **4) Discussion and recommendations**

481 For this Arabian Peninsula event, horizontal resolution in the WRF-Chem model has a considerable effect on the

482 dust budget of the region. Because aerosol prediction models and GCMs still employ cumulus parameterizations, it

483 is important to discuss the uncertainties unearthed in this paper, as well as recommendations for past and future

484 forecasts and research that will be generated prior to our ability to consistently run these models at convection-

485 permitting resolutions.

486 In an average sense, there will be higher dust concentrations produced in convection-permitting simulations

487 compared to those with parameterized convection. The major point here is that the uncertainty in dust concentrations

488 for simulations using different cumulus parameterizations (15 km ensemble), or using different horizontal

489 resolutions with the same cumulus parameterizations (45 km versus 15 km) is small relative to the differences

490 between the use of parameterized versus convection-allowing scales. *Most of the uncertainty in the model's*

491 *predicted dust concentrations comes from the choice to either parameterize convection or run at convection-*

492 *permitting scales.*

493 The results of this research do not stand alone in the literature focused on the impact of horizontal model resolution

494 on dust emissions, and there are several similarities and differences to note when comparing this paper to previous

495 studies. Firstly, concerning the diurnal variation in dust emissions, we find a similar response in the NLLJ

496 mechanism to that of Heinhold et al. (2013) and Marsham et al. (2011), whereby the coarsest simulations

497 overestimate the early morning windspeeds caused by the mixing of the jet to the surface and fail to capture the late

498 afternoon / early evening convective dust lofting mechanism. In these previous studies, the convection-allowing

499 simulation reduces the importance of the NLLJ and enhances the convective maximum, but still retains the NLLJ as

500 the dominant process for dust uplift. Overall, Heinhold et al. (2013) and Marsham et al. (2011) found a net reduction

501 in dust uplift while running at convection-permitting scales. While the NLLJ mechanism is found to be similar here,

502 the analysis reveals an opposite response in WRF-Chem for the Arabian Peninsula, in which the convective

503 maximum dominates, but the NLLJ is still an important mechanism, which thereby leads to more, rather than less

504 dust in the convection-allowing simulations. The net increase in dust concentrations in WRF-Chem is similar to the

505 findings of Reinfried et al. (2009), although Reinfried et al. (2009) focused mainly on haboobs, which may point to

506 convection being the source of agreement rather than the balance between the NLLJ and convection. At this point,

507 we cannot determine whether the discrepancies between our results and previous literature comes from regional or

508 case study differences in the importance of these mechanisms to the dust budget, differences in the models'

509 representation of these processes, or a combination of the two. In all, more work needs to be done to investigate the

510 relationship between the NLLJ and subsequent late afternoon convection in dust producing regions, and the

511 representation of this in numerical models.

512   From a vertically integrated viewpoint, for the Arabian Peninsula region it is possible to rudimentarily tune the dust

513   concentrations of the coarse simulations to that of the convection-permitting simulation by multiplying by an

514   average constant derived from the dust difference plots in Fig. 6-7, which would be on the order of ~2. This is an

515   offline solution, which would aid in enhancing the accuracy of a first-order forecast of vertically integrated or

516   surface dust, and/or AOD. This factor would have to be scaled further, since comparison of the WRF-Chem model

517   to AERONET sites and other AOD observations (Saleeby et al. 2019) shows that WRF-Chem underestimates dust

518   under these conditions. Nevertheless, attempting to use this tuning parameter online in the model (i.e. adjusting the

519   tuning constant, C, in Eq. 1) would not reconcile the differences from a dust flux standpoint. Even if more dust were

520   to be emitted from the surface, the parameterized simulations still lack the necessary variability in updrafts and

521   downdrafts, especially updraft strength, to transport the dust upwards and away from the surface, thus

522   misrepresenting the atmospheric lifetime of these particles in the process.

523   Moreover, tuning the dust concentrations will not change the effect horizontal resolution has on the soil

524   characteristics, particularly soil moisture, and hence on the a priori determined threshold wind speeds which are

525   important in calculating dust lofting in the first place (Fig. 4). If dust concentrations are inaccurately predicted in the

526   coarse simulations, or erroneously tuned, the higher-order online feedbacks will also be incorrect, such as

527   modifications to the radiative budget, and feedbacks to the thermodynamic profile, static stability and mesoscale

528   features, particularly those driven by differences in thermodynamic gradients, such as sea breezes and cold pool

529   propagation.

530   **5) Conclusions**

531   In this study, we have quantified the response sign and magnitude in modeled dust fields in the WRF-Chem regional

532   model to increasing horizontal resolution and the manner in which convection is represented for a summertime

533   Arabian Peninsula event. We have investigated the variability in dust concentrations and fluxes due to the choice of

534   convective parameterization, the representation of convection in the model (explicit versus parameterized), and the

535   effect these differences in dust concentrations have on aerosol heating rates. The case study was simulated at three

536   different horizontal resolutions (45 km, 15 km, and 3 km), with the two coarsest simulations run with cumulus

537   parameterizations, and the 3 km simulation run at convection-permitting resolution. To understand the uncertainty

538   across different parameterizations, five separate cumulus parameterizations were tested in an ensemble (BMJ, AS,

539   GD, TD, KF) at 15 km grid spacing.

540   The convection-allowing simulation exhibited a stronger potential for dust uplift as a function of modeled wind

541   speed, wind threshold, and the location of dust sources. The wind threshold for dust lofting in the 3 km simulation

542   was on average, lower than that for the 15 km or 45 km. This is due to differences in grid resolution leading to

543   changes in the soil moisture, whereby the 3 km simulation displays lower soil wetness across the domain.

544   Furthermore, a distinct difference across simulations was identified in the representation of the bimodal daily

545   maximum in dust emissions in the local mid-morning (mixing of the NLLJ to the surface) and late afternoon

546 (convective outflow boundaries). Compared to the 3 km case, the 45 km simulation overestimates the contribution

547 from the NLLJ and underestimates the role of convection in dust emissions.

548 The 3 km simulation also produced higher vertically integrated dust values at every timestep, as well as higher dust

549 concentrations at every vertical level in the lower troposphere (below 6 km AGL). The uncertainty in dust

550 concentrations for simulations using different cumulus parameterizations (15 km ensemble spread) is much smaller

551 than the difference between the parameterized and convection-permitting convection cases. For the WRF-Chem

552 Arabian Peninsula simulations, the modeled dust fields were most sensitive to the choice of parametrizing or

553 explicitly resolving convective processes. The enhanced dust concentrations in the convection-allowing case are the

554 result of stronger downdrafts lofting more dust from the surface, and stronger updrafts carrying dust to higher levels

555 of the atmosphere, thereby increasing the airborne lifetime of the dust particles. The difference in dust mass across

556 the simulations leads to a significant modification of the radiation budget, specifically the aerosol heating rate. The

557 convection-allowing simulation revealed a greater shortwave and longwave effect, and for aerosol heating rates in

558 the lowest levels, shortwave cooling is stronger than longwave heating, leading to a net cooling effect. Conversely,

559 the opposite radiative response is present in the parameterized cases, resulting in a net warming effect, causing a

560 change in sign in the lowest levels compared to the convection-permitting case.

561 There are a number of implications these results may have on forecasting and future studies. The dust concentrations

562 in the coarse simulations could be tuned offline to match those in the convection-allowing simulation using the

563 percentage difference plots included in Fig. 5-6. This tuning would be on the order of ~2. However, because vertical

564 transport is essential to the vertical concentrations and lifetime of the particles, this tuning factor cannot be applied

565 online. Even if such a tuning were applied, this change will not accurately capture higher-order feedbacks to the

566 meteorology, thermodynamic environment and radiation budget of the Arabian Peninsula, or to the soil moisture

567 wind threshold velocities. Finally, this work also points to the need to better constrain dust concentrations in

568 numerical models, and further develop our understanding of the relationship between storm dynamics and dust

569 processes.

570 **Author contributions**

571 Jennie Bukowski (JB) and Susan C. van den Heever (SvdH) designed the experiments. JB set up and performed the

572 WRF-Chem simulations and wrote the analysis code. Both JB and SvdH contributed to the analysis of the model

573 output. JB prepared the manuscript with contributions and edits from SvdH.

574 **Competing interests**

575 The authors declare that they have no conflict of interest.

576 **Acknowledgements**

577 This work was funded by an Office of Naval Research – Multidisciplinary University Research Initiative (ONR-
578 MURI) grant (# N00014-16-1-2040). Jennie Bukowski was partially supported by the Cooperative Institute for
579 Research in the Atmosphere (CIRA) Program of Research and Scholarly Excellence (PRSE) fellowship. The
580 simulation data are available upon request from the corresponding author, Jennie Bukowski. Initialization data for
581 the model was provided by: National Centers for Environmental Prediction, National Weather Service, NOAA, U.S.
582 Department of Commerce. 2000, updated daily. NCEP FNL Operational Model Global Tropospheric Analyses,
583 continuing from July 1999. Research Data Archive at the National Center for Atmospheric Research, Computational
584 and Informational Systems Laboratory. https://doi.org/10.5065/D6M043C6.

References

586 Alizadeh Choobari, O., Zawar-Reza, P., and Sturman, A.: Low level jet intensification by mineral dust aerosols,
587   Ann. Geophys., 31, 625–632, doi:10.5194/angeo-31-625-2013, 2013.

588 Almazroui, M.: Calibration of TRMM rainfall climatology over Saudi Arabia during 1998–2009, Atmos. Res.,
589   99(3–4), 400–414, doi:10.1016/J.ATMOSRES.2010.11.006, 2011.

590 Aoki, T., Tanaka, T. Y., Uchiyama, A., Chiba, M., Mikami, M., Yabuki, S. And Key, J. R.: Sensitivity Experiments
591   of Direct Radiative Forcing Caused by Mineral Dust Simulated with a Chemical Transport Model, J.
592   Meteorol. Soc. Japan. Ser. II, 83A, 315–331, doi:10.2151/jmsj.83A.315, 2005.

593 Arakawa, A. and Schubert, W. H.: Interaction of a Cumulus Cloud Ensemble with the Large-Scale Environment,
594   Part I, J. Atmos. Sci., 31(3), 674–701, doi:10.1175/1520-0469(1974)031<0674:IOACCE>2.0.CO;2, 1974.

595 Babu, C. A., Jayakrishnan, P. R. and Varikoden, H.: Characteristics of precipitation pattern in the Arabian Peninsula
596   and its variability associated with ENSO, Arab. J. Geosci., 9(3), 186, doi:10.1007/s12517-015-2265-x,
597   2016.

598 Baddock, M. C., Strong, C. L., Leys, J. F., Heidenreich, S. K., Tews, E. K. and McTainsh, G. H.: A visibility and
599   total suspended dust relationship, Atmos. Environ., 89, 329–336, doi:10.1016/J.ATMOSENV.2014.02.038,
600   2014.

601 Barnard, J. C., Fast, J. D., Paredes-Miranda, G., Arnott, W. P. and Laskin, A.: Technical Note: Evaluation of the
602   WRF-Chem "Aerosol Chemical to Aerosol Optical Properties Module" using data from the MILAGRO
603   campaign, Atmos. Chem. Phys., 10(15), 7325–7340, doi:10.5194/acp-10-7325-2010, 2010.

604 Beegum, S. N., Gherboudj, I., Chaouch, N., Temimi, M. and Ghedira, H.: Simulation and analysis of synoptic scale
605   dust storms over the Arabian Peninsula, Atmos. Res., 199, 62–81, doi:10.1016/J.ATMOSRES.2017.09.003,
606   2018.

607 Benedetti, A., Reid, J. S., Knippertz, P., Marsham, J. H., Di Giuseppe, F., Rémy, S., Basart, S., Boucher, O., Brooks,
608   I. M., Menut, L., Mona, L., Laj, P., Pappalardo, G., Wiedensohler, A., Baklanov, A., Brooks, M., Colarco,
609   P. R., Cuevas, E., da Silva, A., Escribano, J., Flemming, J., Huneeus, N., Jorba, O., Kazadzis, S., Kinne, S.,
610   Popp, T., Quinn, P. K., Sekiyama, T. T., Tanaka, T. and Terradellas, E.: Status and future of numerical
611   atmospheric aerosol prediction with a focus on data requirements, Atmos. Chem. Phys., 18(14), 10615–
612   10643, doi:10.5194/acp-18-10615-2018, 2018.

613   Benedetti, A., Baldasano, J. M., Basart, S., Benincasa, F., Boucher, O., Brooks, M. E., Chen, J.-P., Colarco, P. R.,

614   Gong, S., Huneeus, N., Jones, L., Lu, S., Menut, L., Morcrette, J.-J., Mulcahy, J., Nickovic, S., Pérez

615   García-Pando, C., Reid, J. S., Sekiyama, T. T., Tanaka, T. Y., Terradellas, E., Westphal, D. L., Zhang, X.-

616   Y. and Zhou, C.-H.: Operational Dust Prediction, in Mineral Dust: A Key Player in the Earth System,

617   edited by P. Knippertz and J.-B. W. Stuut, pp. 223–265, Springer Netherlands, Dordrecht., 2014.

618   Benedetti, A., Reid, J. S. and Colarco, P. R.: International Cooperative for Aerosol Prediction Workshop on Aerosol

619   Forecast Verification, Bull. Am. Meteorol. Soc., 92(11), ES48-ES53, doi:10.1175/BAMS-D-11-00105.1,

620   2011.

621   Bishop, J. K. B., Davis, R. E. and Sherman, J. T.: Robotic Observations of Dust Storm Enhancement of Carbon

622   Biomass in the North Pacific, Science (80-.)., 298(5594), 817 LP-821, doi:10.1126/science.1074961, 2002.

623   Boose, Y., Welti, A., Atkinson, J., Ramelli, F., Danielczok, A., Bingemer, H. G., Plötze, M., Sierau, B., Kanji, Z. A.

624   and Lohmann, U.: Heterogeneous ice nucleation on dust particles sourced from nine~deserts worldwide --

625   Part 1: Immersion freezing, Atmos. Chem. Phys., 16(23), 15075–15095, doi:10.5194/acp-16-15075-2016,

626   2016.

627   Bouet, C., Cautenet, G., Bergametti, G., Marticorena, B., Todd, M. C. and Washington, R.: Sensitivity of desert dust

628   emissions to model horizontal grid spacing during the Bodélé Dust Experiment 2005, Atmos. Environ., 50,

629   377–380, doi:10.1016/J.ATMOSENV.2011.12.037, 2012.

630   Bryan, G. H., and Morrison, H.: Sensitivity of a Simulated Squall Line to Horizontal Resolution and

631   Parameterization of Microphysics, MWR, 140, 202-225, doi:10.1175/MWR-D-11-00046.1, 2012.

632   Camino, C., Cuevas, E., Basart, S., Alonso-Pérez, S., Baldasano, J. M., Terradellas, E., Marticorena, B., Rodríguez,

633   S. and Berjón, A.: An empirical equation to estimate mineral dust concentrations from visibility

634   observations in Northern Africa, Aeolian Res., 16, 55–68, doi:10.1016/J.AEOLIA.2014.11.002, 2015.

635   Chou, M.-D. and Suarez, M. J.: Technical Report Series on Global Modeling and Data Assimilation A Thermal

636   Infrared Radiation Parameterization for Atmospheric Studies Revised May 2003, Nasa Tech. Memo. 15,

637   NASA, 40 pp., 1999.

638   Corr, C. A., Ziemba, L. D., Scheuer, E., Anderson, B. E., Beyersdorf, A. J., Chen, G., Crosbie, E., Moore, R. H.,

639   Shook, M., Thornhill, K. L., Winstead, E., Lawson, R. P., Barth, M. C., Schroeder, J. R., Blake, D. R. and

640   Dibb, J. E.: Observational evidence for the convective transport of dust over the Central United States, J.

641   Geophys. Res. Atmos., 121(3), 1306–1319, doi:10.1002/2015JD023789, 2016.

642   Cowie, S. M., Marsham, J. H. and Knippertz, P.: The importance of rare, high-wind events for dust uplift in northern

643   Africa, Geophys. Res. Lett., 42(19), 8208–8215, doi:10.1002/2015GL065819, 2015.

644   Dayan, U., Ziv, B., Margalit, A., Morin, E. and Sharon, D.: A severe autumn storm over the middle-east: synoptic

645   and mesoscale convection analysis, Theor. Appl. Climatol., 69(1), 103–122, doi:10.1007/s007040170038,

646   2001.

647   Dipu, S., Prabha, T. V., Pandithurai, G., Dudhia, J., Pfister, G., Rajesh, K. and Goswami, B. N.: Impact of elevated

648   aerosol layer on the cloud macrophysical properties prior to monsoon onset, Atmos. Environ., 70, 454–467,

649   doi:10.1016/J.ATMOSENV.2012.12.036, 2013.

650   Emmons, L. K., Walters, S., Hess, P. G., Lamarque, J.-F., Pfister, G. G., Fillmore, D., Granier, C., Guenther,

651   A., Kinnison, D., Laepple, T., Orlando, J., Tie, X., Tyndall, G., Wiedinmyer, C., Baughcum, S. L., and

652   Kloster, S.: Description and evaluation of the Model for Ozone and Related chemical Tracers, version 4

653   (MOZART-4), Geosci. Model Dev., 3, 43-67, doi.org/10.5194/gmd-3-43-2010, 2010. *We acknowledge use*

654   *of NCAR/ACOM CAM-chem global model output available at [https://www.acom.ucar.edu/cam-chem/cam-](https://www.acom.ucar.edu/cam-chem/cam-chem.shtml)*

655   *[chem.shtml](https://www.acom.ucar.edu/cam-chem/cam-chem.shtml)*.

656

657   Fadnavis, S., Semeniuk, K., Pozzoli, L., Schultz, M. G., Ghude, S. D., Das, S. and Kakatkar, R.: Transport of

658   aerosols into the UTLS and their impact on the Asian monsoon region as seen in a global model simulation,

659   Atmos. Chem. Phys., 13(17), 8771–8786, doi:10.5194/acp-13-8771-2013, 2013.

660   Fast, J. D., Gustafson Jr., W. I., Easter, R. C., Zaveri, R. A., Barnard, J. C., Chapman, E. G., Grell, G. A. and

661   Peckham, S. E.: Evolution of ozone, particulates, and aerosol direct radiative forcing in the vicinity of

662   Houston using a fully coupled meteorology-chemistry-aerosol model, J. Geophys. Res. Atmos., 111(D21),

663   doi:10.1029/2005JD006721, 2006.

664   Field, P. R., Möhler, O., Connolly, P., Krämer, M., Cotton, R., Heymsfield, A. J., Saathoff, H. and Schnaiter, M.:

665   Some ice nucleation characteristics of Asian and Saharan desert dust, Atmos. Chem. Phys., 6(10), 2991–

666   3006, doi:10.5194/acp-6-2991-2006, 2006.

667   Giannakopoulou, E. M. and Toumi, R.: The Persian Gulf summertime low-level jet over sloping terrain, Q. J. R.

668   Meteorol. Soc., 138(662), 145–157, doi:10.1002/qj.901, 2012.

669   Ginoux, P., Chin, M., Tegen, I., Prospero, J. M., Holben, B., Dubovik, O. and Lin, S.-J.: Sources and distributions of

670   dust aerosols simulated with the GOCART model, J. Geophys. Res. Atmos., 106(D17), 20255–20273,

671   doi:10.1029/2000JD000053, 2001.

672   Ginoux, P., Prospero, J. M., Gill, T. E., Hsu, N. C. and Zhao, M.: Global-scale attribution of anthropogenic and

673   natural dust sources and their emission rates based on MODIS Deep Blue aerosol products, Rev. Geophys.,

674   50(3), doi:10.1029/2012RG000388, 2012.

675   Grell, G. A., Peckham, S. E., Schmitz, R., McKeen, S. A., Frost, G., Skamarock, W. C. and Eder, B.: Fully coupled

676   "online" chemistry within the WRF model, Atmos. Environ., 39(37), 6957–6975,

677   doi:10.1016/J.ATMOSENV.2005.04.027, 2005.

678   Hasanean, H., Almazroui, M., Hasanean, H. and Almazroui, M.: Rainfall: Features and Variations over Saudi

679   Arabia, A Review, Climate, 3(3), 578–626, doi:10.3390/cli3030578, 2015.

680   Haywood, J. M., Allan, R. P., Culverwell, I., Slingo, T., Milton, S., Edwards, J. and Clerbaux, N.: Can desert dust

681   explain the outgoing longwave radiation anomaly over the Sahara during July 2003?, J. Geophys. Res.

682   Atmos., 110(D5), doi:10.1029/2004JD005232, 2005.

683   Heald, C. L., Ridley, D. A., Kroll, J. H., Barrett, S. R. H., Cady-Pereira, K. E., Alvarado, M. J. and Holmes, C. D.:

684   Contrasting the direct radiative effect and direct radiative forcing of aerosols, Atmos. Chem. Phys., 14(11),

685   5513–5527, doi:10.5194/acp-14-5513-2014, 2014.

686   Heinold, B., Knippertz, P., Marsham, J. H., Fiedler, S., Dixon, N. S., Schepanski, K., Laurent, B. and Tegen, I.: The

687   role of deep convection and nocturnal low-level jets for dust emission in summertime West Africa:

688   Estimates from convection-permitting simulations, J. Geophys. Res. Atmos., 118(10), 4385–4400,

689   doi:10.1002/jgrd.50402, 2013.

690 Huneeus, N., Schulz, M., Balkanski, Y., Griesfeller, J., Prospero, J., Kinne, S., Bauer, S., Boucher, O., Chin, M.,

691   Dentener, F., Diehl, T., Easter, R., Fillmore, D., Ghan, S., Ginoux, P., Grini, A., Horowitz, L., Koch, D.,

692   Krol, M. C., Landing, W., Liu, X., Mahowald, N., Miller, R., Morcrette, J.-J., Myhre, G., Penner, J.,

693   Perlwitz, J., Stier, P., Takemura, T. and Zender, C. S.: Global dust model intercomparison in AeroCom

694   phase I, Atmos. Chem. Phys., 11(15), 7781–7816, doi:10.5194/acp-11-7781-2011, 2011.

695 Jickells, T. and Moore, C. M.: The Importance of Atmospheric Deposition for Ocean Productivity, Annu. Rev. Ecol.

696   Evol. Syst., 46(1), 481–501, doi:10.1146/annurev-ecolsys-112414-054118, 2015.

697 Jish Prakash, P., Stenchikov, G., Kalenderski, S., Osipov, S. and Bangalath, H.: The impact of dust storms on the

698   Arabian Peninsula and the Red Sea, Atmos. Chem. Phys., 15(1), 199–222, doi:10.5194/acp-15-199-2015,

699   2015.

700 Jung, E., Shao, Y. and Sakai, T.: A study on the effects of convective transport on regional-scale Asian dust storms

701   in 2002, J. Geophys. Res. Atmos., 110(D20), doi:10.1029/2005JD005808, 2005.

702 Kain, J. S.: The Kain–Fritsch Convective Parameterization: An Update, J. Appl. Meteorol., 43(1), 170–181,

703   doi:10.1175/1520-0450(2004)043<0170:TKCPAU>2.0.CO;2, 2004.

704 Kalenderski, S., Stenchikov, G. and Zhao, C.: Modeling a typical winter-time dust event over the Arabian Peninsula

705   and the Red Sea, Atmos. Chem. Phys., 13(4), 1999–2014, doi:10.5194/acp-13-1999-2013, 2013.

706 Kalenderski, S. and Stenchikov, G.: High-resolution regional modeling of summertime transport and impact of

707   African dust over the Red Sea and Arabian Peninsula, J. Geophys. Res. Atmos., 121(11), 6435–6458,

708   doi:10.1002/2015JD024480, 2016.

709 Karydis, V. A., Kumar, P., Barahona, D., Sokolik, I. N. and Nenes, A.: On the effect of dust particles on global

710   cloud condensation nuclei and cloud droplet number, J. Geophys. Res. Atmos., 116(D23),

711   doi:10.1029/2011JD016283, 2011.

712 Kinne, S., Lohmann, U., Feichter, J., Schulz, M., Timmreck, C., Ghan, S., Easter, R., Chin, M., Ginoux, P.,

713   Takemura, T., Tegen, I., Koch, D., Herzog, M., Penner, J., Pitari, G., Holben, B., Eck, T., Smirnov, A.,

714   Dubovik, O., Slutsker, I., Tanre, D., Torres, O., Mishchenko, M., Geogdzhayev, I., Chu, D. A. and

715   Kaufman, Y.: Monthly averages of aerosol properties: A global comparison among models, satellite data,

716   and AERONET ground data, J. Geophys. Res. Atmos., 108(D20), doi:10.1029/2001JD001253, 2003.

717 Kishcha, P., Alpert, P., Barkan, J., Kirschner, I. and Machenhauer, B.: Atmospheric response to Saharan dust

718   deduced from ECMWF reanalysis (ERA) temperature increments, Tellus B Chem. Phys. Meteorol., 55(4),

719   901–913, doi:10.3402/tellusb.v55i4.16380, 2011.

720 Klich, C. A. and Fuelberg, H. E.: The role of horizontal model resolution in assessing the transport of CO in a

721   middle latitude cyclone using WRF-Chem, Atmos. Chem. Phys., 14(2), 609–627, doi:10.5194/acp-14-609-

722   2014, 2014.

723 Klose, M. and Shao, Y.: Stochastic parameterization of dust emission and application to convective atmospheric

724   conditions, Atmos. Chem. Phys., 12, 7309-7320, doi:10.5194/acp-12-7309-2012, 2012.

725   Knopf, D. A. and Koop, T.: Heterogeneous nucleation of ice on surrogates of mineral dust, J. Geophys. Res. Atmos.,

726   111(D12), doi:10.1029/2005JD006894, 2006.

727   Kok, J. F., Mahowald, N. M., Fratini, G., Gillies, J. A., Ishizuka, M., Leys, J. F., Mikami, M., Park, M.-S., Park, S.-

728   U., Van Pelt, R. S. and Zobeck, T. M.: An improved dust emission model – Part 1: Model description and

729   comparison against measurements, Atmos. Chem. Phys., 14(23), 13023–13041, doi:10.5194/acp-14-13023-

730   2014, 2014.

731   Kok, J. F., Ward, D. S., Mahowald, N. M. and Evan, A. T.: Global and regional importance of the direct dust-

732   climate feedback, Nat. Commun., 9(1), 241, doi:10.1038/s41467-017-02620-y, 2018.

733   Largeron, Y., Guichard, F., Bouniol, D., Couvreux, F., Kergoat, L. and Marticorena, B.: Can we use surface wind

734   fields from meteorological reanalyses for Sahelian dust emission simulations?, Geophys. Res. Lett., 42(7),

735   2490–2499, doi:10.1002/2014GL062938, 2015.

736   Lee, Y. H., Chen, K. and Adams, P. J.: Development of a global model of mineral dust aerosol microphysics,

737   Atmos. Chem. Phys., 9(7), 2441–2458, doi:10.5194/acp-9-2441-2009, 2009.

738   Liao, H. and Seinfeld, J. H.: Radiative forcing by mineral dust aerosols: Sensitivity to key variables, J. Geophys.

739   Res. Atmos., 103(D24), 31637–31645, doi:10.1029/1998JD200036, 1998.

740   Mahowald, N. M., Ballantine, J. A., Feddema, J. and Ramankutty, N.: Global trends in visibility: implications for

741   dust sources, Atmos. Chem. Phys., 7(12), 3309–3339, doi:10.5194/acp-7-3309-2007, 2007.

742   Mahowald, N. M., Baker, A. R., Bergametti, G., Brooks, N., Duce, R. A., Jickells, T. D., Kubilay, N., Prospero, J.

743   M. and Tegen, I.: Atmospheric global dust cycle and iron inputs to the ocean, Global Biogeochem. Cycles,

744   19(4), doi:10.1029/2004GB002402, 2005.

745   Manktelow, P. T., Carslaw, K. S., Mann, G. W. and Spracklen, D. V: The impact of dust on sulfate aerosol, CN and

746   CCN during an East Asian dust storm, Atmos. Chem. Phys., 10(2), 365–382, doi:10.5194/acp-10-365-

747   2010, 2010.

748   Marsham, J. H., Parker, D. J., Grams, C. M., Taylor, C. M. and Haywood, J. M.: Uplift of Saharan dust south of the

749   intertropical discontinuity, J. Geophys. Res. Atmos., 113(D21), doi:10.1029/2008JD009844, 2008.

750   Marsham, J. H., Knippertz, P., Dixon, N. S., Parker, D. J. and Lister, G. M. S.: The importance of the representation

751   of deep convection for modeled dust-generating winds over West Africa during summer, Geophys. Res.

752   Lett., 38(16), doi:10.1029/2011GL048368, 2011.

753   Marticorena, B. and Bergametti, G.: Modeling the atmospheric dust cycle: 1. Design of a soil-derived dust emission

754   scheme, J. Geophys. Res. Atmos., 100(D8), 16415–16430, doi:10.1029/95JD00690, 1995.

755   Martin, J. H.: Iron still comes from above, Nature, 353(6340), 123, doi:10.1038/353123b0, 1991.

756   Miller, S. D., Grasso, L., Bian, Q., Kreidenweis, S., Dostalek, J., Solbrig, J., Bukowski, J., van den Heever, S. C.,

757   Wang, Y., Xu, X., Wang, J., Walker, A., Wu, T.-C., Zupanski, M., Chiu, C., and Reid, J.: *A Tale of Two*

758   *Dust Storms*: Analysis of a Complex Dust Event in the Middle East, Atmos. Meas. Tech. Discuss.,

759   doi:10.5194/amt-2019-82, 2019.

760   Miller, S. D., Kuciauskas, A. P., Liu, M., Ji, Q., Reid, J. S., Breed, D. W., Walker, A. L. and Mandoos, A. Al:

761   Haboob dust storms of the southern Arabian Peninsula, J. Geophys. Res. Atmos., 113(D1),

762   doi:10.1029/2007JD008550, 2008.

763   Morrison, H., Curry, J. A. and Khvorostyanov, V. I.: A New Double-Moment Microphysics Parameterization for

764   Application in Cloud and Climate Models. Part I: Description, J. Atmos. Sci., 62(6), 1665–1677,

765   doi:10.1175/JAS3446.1, 2005.

766   Morrison, H., Thompson, G. and Tatarskii, V.: Impact of Cloud Microphysics on the Development of Trailing

767   Stratiform Precipitation in a Simulated Squall Line: Comparison of One- and Two-Moment Schemes, Mon.

768   Weather Rev., 137(3), 991–1007, doi:10.1175/2008MWR2556.1, 2009.

769   Nakanishi, M. and Niino, H.: An Improved Mellor--Yamada Level-3 Model: Its Numerical Stability and Application

770   to a Regional Prediction of Advection Fog, Boundary-Layer Meteorol., 119(2), 397–407,

771   doi:10.1007/s10546-005-9030-8, 2006.

772   Nakanishi, M. and NIINO, H.: Development of an Improved Turbulence Closure Model for the Atmospheric

773   Boundary Layer, J. Meteorol. Soc. Japan. Ser. II, 87(5), 895–912, doi:10.2151/jmsj.87.895, 2009.

774   National Centers for Environmental Prediction/National Weather Service/NOAA/U.S. Department of Commerce:

775   NCEP GDAS/FNL 0.25 Degree Global Tropospheric Analyses and Forecast Grids, Research Data Archive

776   at the National Center for Atmospheric Research, Computational and Information Systems Laboratory,

777   Boulder, CO, https://doi.org/10.5065/D65Q4T4Z, 2015.

778   Niu, G.-Y., Yang, Z.-L., Mitchell, K. E., Chen, F., Ek, M. B., Barlage, M., Kumar, A., Manning, K., Niyogi, D.,

779   Rosero, E., Tewari, M. and Xia, Y.: The community Noah land surface model with multiparameterization

780   options (Noah-MP): 1. Model description and evaluation with local-scale measurements, J. Geophys. Res.

781   Atmos., 116(D12), doi:10.1029/2010JD015139, 2011.

782   Pantillon, F., Knippertz, P., Marsham, J. H. and Birch, C. E.: A Parameterization of Convective Dust Storms for

783   Models with Mass-Flux Convection Schemes, J. Atmos. Sci., 72(6), 2545–2561, doi:10.1175/JAS-D-14-

784   0341.1, 2015.

785   Pantillon, F., Knippertz, P., Marsham, J. H., Panitz, H.-J. and Bischoff-Gauss, I.: Modeling haboob dust storms in

786   large-scale weather and climate models, J. Geophys. Res. Atmos., 121(5), 2090–2109,

787   doi:10.1002/2015JD024349, 2016.

788   Pérez, C., Nickovic, S., Pejanovic, G., Baldasano, J. M. and Özsoy, E.: Interactive dust-radiation modeling: A step

789   to improve weather forecasts, J. Geophys. Res. Atmos., 111(D16), doi:10.1029/2005JD006717, 2006.

790   Pope, R. J., Marsham, J. H., Knippertz, P., Brooks, M. E. and Roberts, A. J.: Identifying errors in dust models from

791   data assimilation, Geophys. Res. Lett., 43(17), 9270–9279, doi:10.1002/2016GL070621, 2016.

792   Prospero, J. M.: Long-term measurements of the transport of African mineral dust to the southeastern United States:

793   Implications for regional air quality, J. Geophys. Res. Atmos., 104(D13), 15917–15927,

794   doi:10.1029/1999JD900072, 1999.

795   Reid, J. S., Benedetti, A., Colarco, P. R. and Hansen, J. A.: International Operational Aerosol Observability

796   Workshop, Bull. Am. Meteorol. Soc., 92(6), ES21-ES24, doi:10.1175/2010BAMS3183.1, 2010.

797   Reinfried, F., Tegen, I., Heinold, B., Hellmuth, O., Schepanski, K., Cubasch, U., Huebener, H. and Knippertz, P.:

798   Simulations of convectively-driven density currents in the Atlas region using a regional model: Impacts on

799   dust emission and sensitivity to horizontal resolution and convection schemes, J. Geophys. Res. Atmos.,

800   114(D8), doi:10.1029/2008JD010844, 2009.

801   Ridley, D. A., Heald, C. L., Pierce, J. R. and Evans, M. J.: Toward resolution-independent dust emissions in global

802   models: Impacts on the seasonal and spatial distribution of dust, Geophys. Res. Lett., 40(11), 2873–2877,

803   doi:10.1002/grl.50409, 2013.

804   Roberts, A. J., Woodage, M. J., Marsham, J. H., Highwood, E. J., Ryder, C. L., McGinty, W., Wilson, S., and

805   Crook, J.: Can explicit convection improve modelled dust in summertime West Africa?, Atmos. Chem.

806   Phys., 18, 9025-9048, https://doi.org/10.5194/acp-18-9025-2018, 2018.

807   Saleeby, S. M., van den Heever, S. C., Bukowski, J., Walker, A. L., Solbrig, J. E., Atwood, S. A., Bian, Q.,

808   Kreidenweis, S. M., Wang, Y., Wang, J. and Miller, S. D.: The Influence of Simulated Surface Dust

809   Lofting Erodible Fraction on Radiative Forcing, Atmos. Chem. Phys. Discuss., 2019, 1–35,

810   doi:10.5194/acp-2018-1302, 2019.

811   Schepanski, K., Knippertz, P., Fiedler, S., Timouk, F. and Demarty, J.: The sensitivity of nocturnal low-level jets

812   and near-surface winds over the Sahel to model resolution, initial conditions and boundary-layer set-up.

813   Q.J.R. Meteorol. Soc., 141, 1442-1456. doi:10.1002/qj.2453, 2015.

814   Seigel, R. B. and van den Heever, S. C.: Dust Lofting and Ingestion by Supercell Storms, J. Atmos. Sci., 69(5),

815   1453–1473, doi:10.1175/JAS-D-11-0222.1, 2012.

816   Sessions, W. R., Reid, J. S., Benedetti, A., Colarco, P. R., da Silva, A., Lu, S., Sekiyama, T., Tanaka, T. Y.,

817   Baldasano, J. M., Basart, S., Brooks, M. E., Eck, T. F., Iredell, M., Hansen, J. A., Jorba, O. C., Juang, H.-

818   M. H., Lynch, P., Morcrette, J.-J., Moorthi, S., Mulcahy, J., Pradhan, Y., Razinger, M., Sampson, C. B.,

819   Wang, J. and Westphal, D. L.: Development towards a global operational aerosol consensus: basic

820   climatological characteristics of the International Cooperative for Aerosol Prediction Multi-Model

821   Ensemble (ICAP-MME), Atmos. Chem. Phys., 15(1), 335–362, doi:10.5194/acp-15-335-2015, 2015.

822   Shwehdi, M. H.: Thunderstorm distribution and frequency in Saudi Arabia, J. Geophys. Eng., 2(3), 252–267,

823   doi:10.1088/1742-2132/2/3/009, 2005.

824   Skamarock, W. C., Klemp, J. B., Dudhia, J. O. G. D., and Barker, D. M.: A description of the Advanced Research

825   WRF version 3, NCAR Tech. Note NCAR/TN-4751STR, NCAR, http://dx.doi.org/10.5065/D68S4MVH,

826   Boulder, CO, 2008.

827   Slingo, A., Ackerman, T. P., Allan, R. P., Kassianov, E. I., McFarlane, S. A., Robinson, G. J., Barnard, J. C., Miller,

828   M. A., Harries, J. E., Russell, J. E. and Dewitte, S.: Observations of the impact of a major Saharan dust

829   storm on the atmospheric radiation balance, Geophys. Res. Lett., 33(24), doi:10.1029/2006GL027869,

830   2006.

831   Sokolik, I. N. and Toon, O. B.: Direct radiative forcing by anthropogenic airborne mineral aerosols, Nature,

832   381(6584), 681–683, doi:10.1038/381681a0, 1996.

833   Stafoggia, M., Zauli-Sajani, S., Pey, J., Samoli, E., Alessandrini, E., Basagaña, X., Cernigliaro, A., Chiusolo, M.,

834   Demaria, M., Díaz, J., Faustini, A., Katsouyanni, K., Kelessis, A. G., Linares, C., Marchesi, S., Medina, S.,

835   Pandolfi, P., Pérez, N., Querol, X., Randi, G., Ranzi, A., Tobias, A., Forastiere, F. and null null: Desert

836   Dust Outbreaks in Southern Europe: Contribution to Daily PM_{10} Concentrations and Short-Term

837   Associations with Mortality and Hospital Admissions, Environ. Health Perspect., 124(4), 413–419,

838   doi:10.1289/ehp.1409164, 2016.

839 Stephens, G. L., L'Ecuyer, T., Forbes, R., Gettelmen, A., Golaz, J.-C., Bodas-Salcedo, A., Suzuki, K., Gabriel, P.,

840   and Haynes, J.: Dreary state of precipitation in global models, J. Geophys. Res., 115, D24211,

841   doi:10.1029/2010JD014532, 2010.

842 Sun, Y., Solomon, S., Dai, A., and Portmann, R. W.: How often does it rain? J. Clim., 19, 916–934,

843   doi:10.1175/JCLI3672.1, 2006.

844 Takemi, T.: Importance of the Numerical Representation of Shallow and Deep Convection for Simulations of

845   Dust Transport over a Desert Region, Adv. Meteorol., vol. 2012, 1-13, doi: 10.1155/2012/413584, 2012.

846 Tanaka, T. Y. and Chiba, M.: A numerical study of the contributions of dust source regions to the global dust

847   budget, Glob. Planet. Change, 52(1–4), 88–104, doi:10.1016/J.GLOPLACHA.2006.02.002, 2006.

848 Tegen, I. and Lacis, A. A.: Modeling of particle size distribution and its influence on the radiative properties of

849   mineral dust aerosol, J. Geophys. Res. Atmos., 101(D14), 19237–19244, doi:10.1029/95JD03610, 1996.

850 Teixeira, J. C., Carvalho, A. C., Tuccella, P., Curci, G. and Rocha, A.: WRF-chem sensitivity to vertical resolution

851   during a saharan dust event, Phys. Chem. Earth, Parts A/B/C, 94, 188–195,

852   doi:10.1016/J.PCE.2015.04.002, 2016.

853 Todd, M. C., Bou Karam, D., Cavazos, C., Bouet, C., Heinold, B., Baldasano, J. M., Cautenet, G., Koren, I., Perez,

854   C., Solmon, F., Tegen, I., Tulet, P., Washington, R. and Zakey, A.: Quantifying uncertainty in estimates of

855   mineral dust flux: An intercomparison of model performance over the Bodélé Depression, northern Chad, J.

856   Geophys. Res. Atmos., 113(D24), doi:10.1029/2008JD010476, 2008.

857 Tulet, P., Crahan-Kaku, K., Leriche, M., Aouizerats, B. and Crumeyrolle, S.: Mixing of dust aerosols into a

858   mesoscale convective system: Generation, filtering and possible feedbacks on ice anvils, Atmos. Res.,

859   96(2–3), 302–314, doi:10.1016/J.ATMOSRES.2009.09.011, 2010.

860 Twohy, C. H., Kreidenweis, S. M., Eidhammer, T., Browell, E. V, Heymsfield, A. J., Bansemer, A. R., Anderson, B.

861   E., Chen, G., Ismail, S., DeMott, P. J. and Van Den Heever, S. C.: Saharan dust particles nucleate droplets

862   in eastern Atlantic clouds, Geophys. Res. Lett., 36(1), doi:10.1029/2008GL035846, 2009.

863 Uno, I., Wang, Z., Chiba, M., Chun, Y. S., Gong, S. L., Hara, Y., Jung, E., Lee, S.-S., Liu, M., Mikami, M., Music,

864   S., Nickovic, S., Satake, S., Shao, Y., Song, Z., Sugimoto, N., Tanaka, T. and Westphal, D. L.: Dust model

865   intercomparison (DMIP) study over Asia: Overview, J. Geophys. Res. Atmos., 111(D12),

866   doi:10.1029/2005JD006575, 2006.

867 van Donkelaar, A., Martin, R. V, Brauer, M., Kahn, R., Levy, R., Verduzco, C. and Villeneuve, P. J.: Global

868   estimates of ambient fine particulate matter concentrations from satellite-based aerosol optical depth:

869   development and application, Environ. Health Perspect., 118(6), 847–855, doi:10.1289/ehp.0901623, 2010.

870 Woodage, M. J. and Woodward, S.: U.K. HiGEM: Impacts of Desert Dust Radiative Forcing in a High-Resolution

871   Atmospheric GCM, J. Clim., 27(15), 5907–5928, doi:10.1175/JCLI-D-13-00556.1, 2014.

872 Yang, Q., Easter, R. C., Campuzano-Jost, P., Jimenez, J. L., Fast, J. D., Ghan, S. J., Wang, H., Berg, L. K., Barth,

873   M. C., Liu, Y., Shrivastava, M. B., Singh, B., Morrison, H., Fan, J., Ziegler, C. L., Bela, M., Apel, E.,

874   Diskin, G. S., Mikoviny, T. and Wisthaler, A.: Aerosol transport and wet scavenging in deep convective

875   clouds: A case study and model evaluation using a multiple passive tracer analysis approach, J. Geophys.

876   Res. Atmos., 120(16), 8448–8468, doi:10.1002/2015JD023647, 2015.

877 Yang, Z.-L., Niu, G.-Y., Mitchell, K. E., Chen, F., Ek, M. B., Barlage, M., Longuevergne, L., Manning, K., Niyogi,

878   D., Tewari, M. and Xia, Y.: The community Noah land surface model with multiparameterization options

879   (Noah-MP): 2. Evaluation over global river basins, J. Geophys. Res. Atmos., 116(D12),

880   doi:10.1029/2010JD015140, 2011.

881 Yin, Y., Chen, Q., Jin, L., Chen, B., Zhu, S. and Zhang, X.: The effects of deep convection on the concentration and

882   size distribution of aerosol particles within the upper troposphere: A case study, J. Geophys. Res. Atmos.,

883   117(D22), doi:10.1029/2012JD017827, 2012.

884 Yu, Y., Notaro, M., Kalashnikova, O. V and Garay, M. J.: Climatology of summer Shamal wind in the Middle East,

885   J. Geophys. Res. Atmos., 121(1), 289–305, doi:10.1002/2015JD024063, 2016.

886 Yuter, S. E. and Houze, R. A.: Three-Dimensional Kinematic and Microphysical Evolution of Florida

887   Cumulonimbus. Part II: Frequency Distributions of Vertical Velocity, Reflectivity, and Differential

888   Reflectivity, Mon. Weather Rev., 123(7), 1941–1963, doi:10.1175/1520-

889   0493(1995)123<1941:TDKAME>2.0.CO;2, 1995.

890 Zender, C. S., Miller, R. L. R. L. and Tegen, I.: Quantifying mineral dust mass budgets:Terminology, constraints,

891   and current estimates, Eos, Trans. Am. Geophys. Union, 85(48), 509–512, doi:10.1029/2004EO480002,

892   2004.

893 Zhao, C., Liu, X., Leung, L. R., Johnson, B., McFarlane, S. A., Gustafson Jr., W. I., Fast, J. D. and Easter, R.: The

894   spatial distribution of mineral dust and its shortwave radiative forcing over North Africa: modeling

895   sensitivities to dust emissions and aerosol size treatments, Atmos. Chem. Phys., 10(18), 8821–8838,

896   doi:10.5194/acp-10-8821-2010, 2010.

897

WRF-Chem Version 3.9.1.1	Parameterization / Model Option
Simulation Start	02-Aug-2016-00:00:00 UTC
Simulation End	05-Aug-2016-00:00:00 UTC
Domains	dx = dy = 45km / 15km / 3km
Nesting	One-way
Vertical Levels	50 stretched
Initialization	GDAS-FNL Reanalysis
Aerosol Module / Erodible Grid Map	GOCART / Ginoux et al. (2004)
Microphysics	Morrison 2-Moment
Radiation	RRTMG Longwave & Goddard Shortwave
Land Surface	Noah-MP Land Surface Model
Cumulus Schemes (45 km and 15 km grids only)	Betts–Miller–Janjic (BMJ)
	Kain–Fritsch (KF)
	Grell 3D Ensemble (GD)
	Tiedtke Scheme (TD)
	Simplified Arakawa–Schubert (AS)
Boundary Layer / Surface Layer	MYNN Level 3

898   **Table 1: Summary of WRF-Chem model options utilized and the simulation setup.**

899
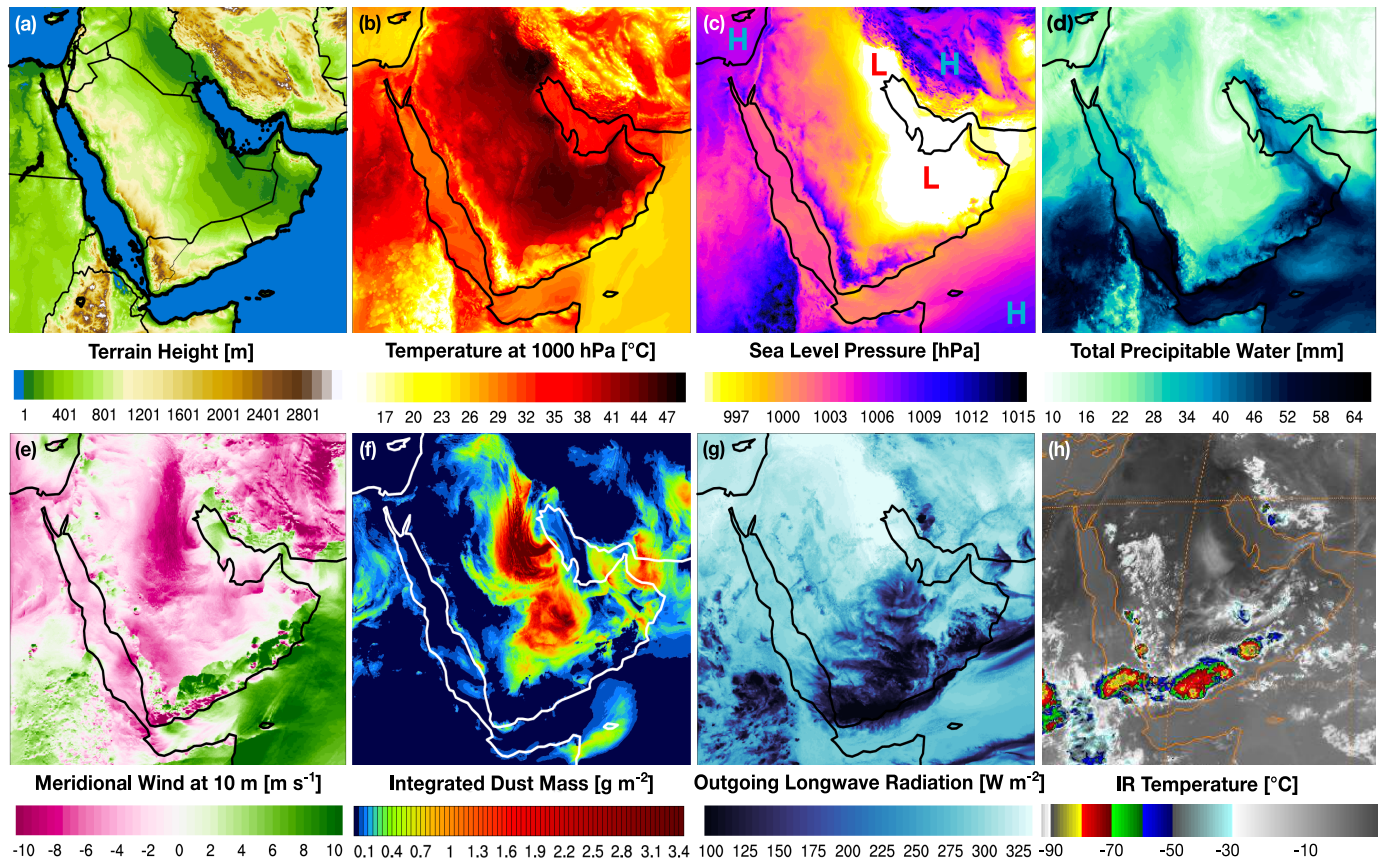
Figure 1: Case study topography and meteorology for August 3, 2016 at 15:00 UTC: (a) terrain height and national

boundaries, (b) 1000 hPa Temperature, (c) sea level pressure, (d) total precipitable water, (e) meridional winds at 10 m

AGL, (f) vertically integrated dust mass, (g) outgoing longwave radiation, and (h) IR temperature. Panel (h) is observed

from Meteosat-7 while panels (a-g) are snapshots from the 3 km WRF-Chem simulation

904
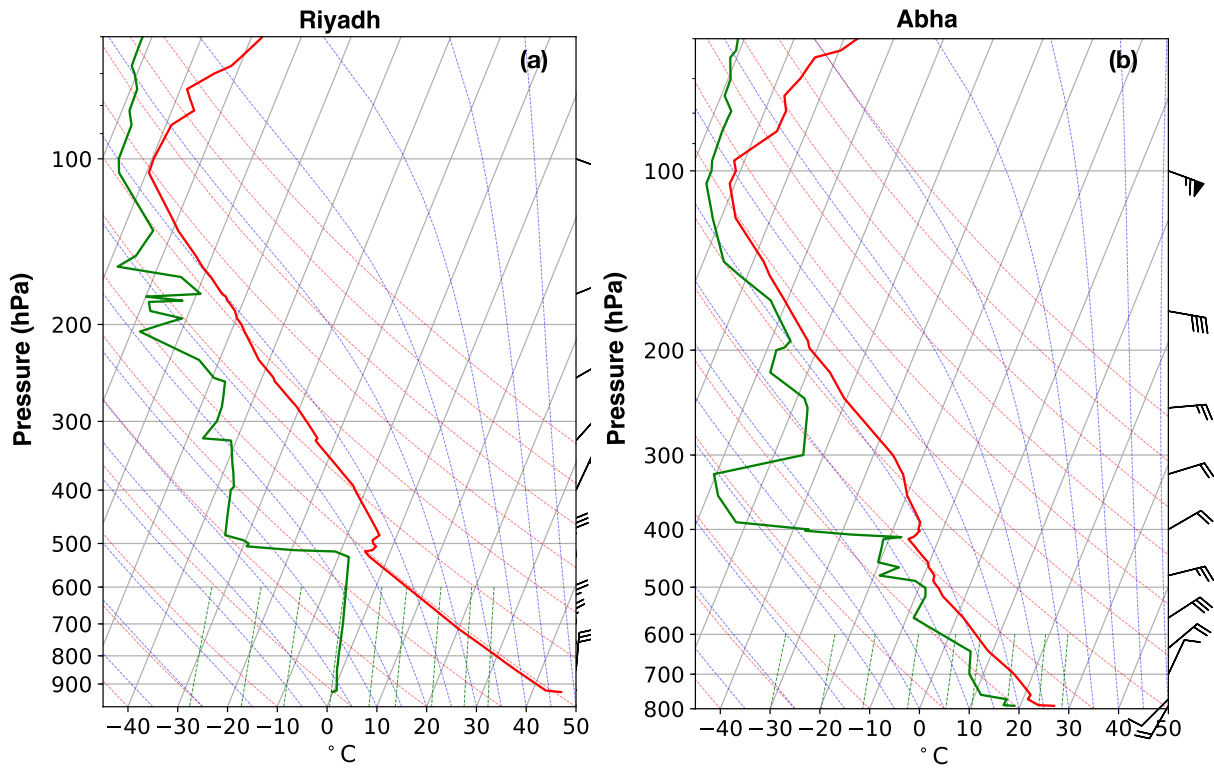
905 **Figure 2. Skew-T diagrams for two radiosonde release sites in Saudi Arabia on August 3, 2016 at 12:00 UTC for an inland**
906 **location (a) and a location nearer to the coast (b).**

907

908
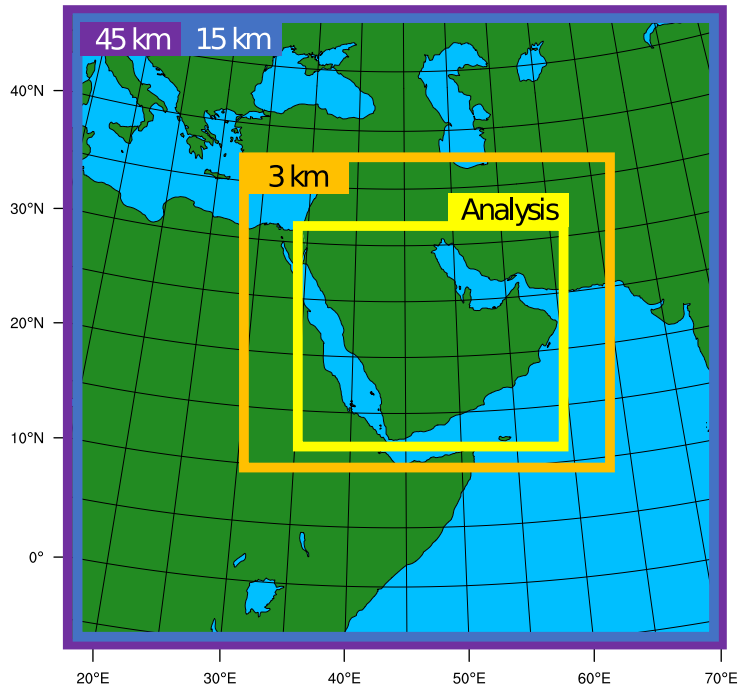
Figure 3: Model domain setup and analysis region for the 45 km (purple) and 15 km (blue) independent simulations with cumulus parameterizations, and the 3 km nested convection permitting simulation (orange). The averaging region for the analysis is denoted in yellow.

912
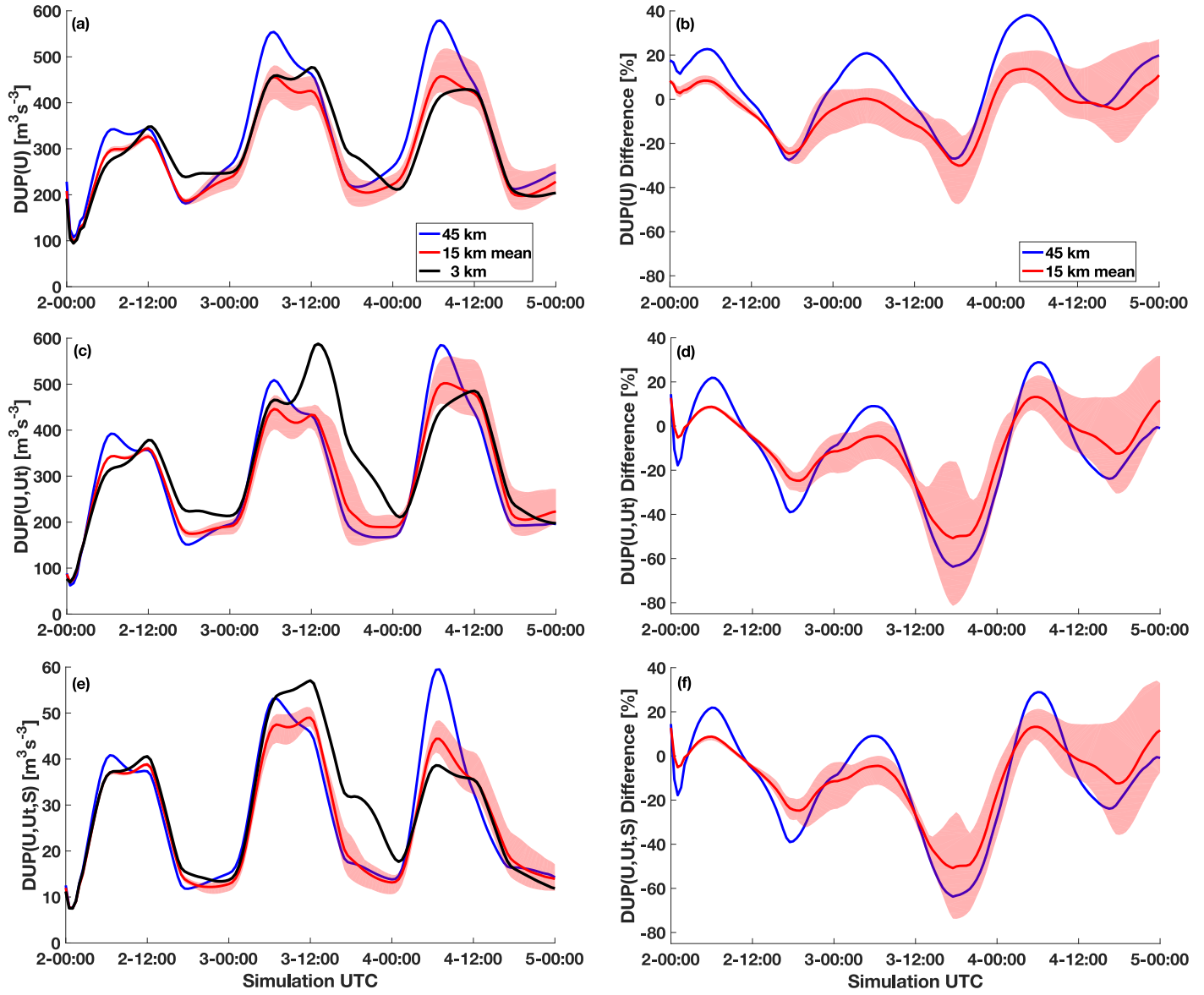
Figure 4: Left column: spatially averaged dust uplift potential for (a) DUP(U), (c) DUP(U,U$_t$), and (e) DUP(U,U$_t$,S) for the 45 km (blue), 15 km mean (red), and 3 km (black) simulations with the maximum and minimum spread across the 15 km simulations indicated in light red shading. Note that in panel (e) there is a change in scale in the ordinate. Right column: percent difference between the 3 km convection-permitting simulation and the simulations employing cumulus parameterizations for the different DUP parameters.

918
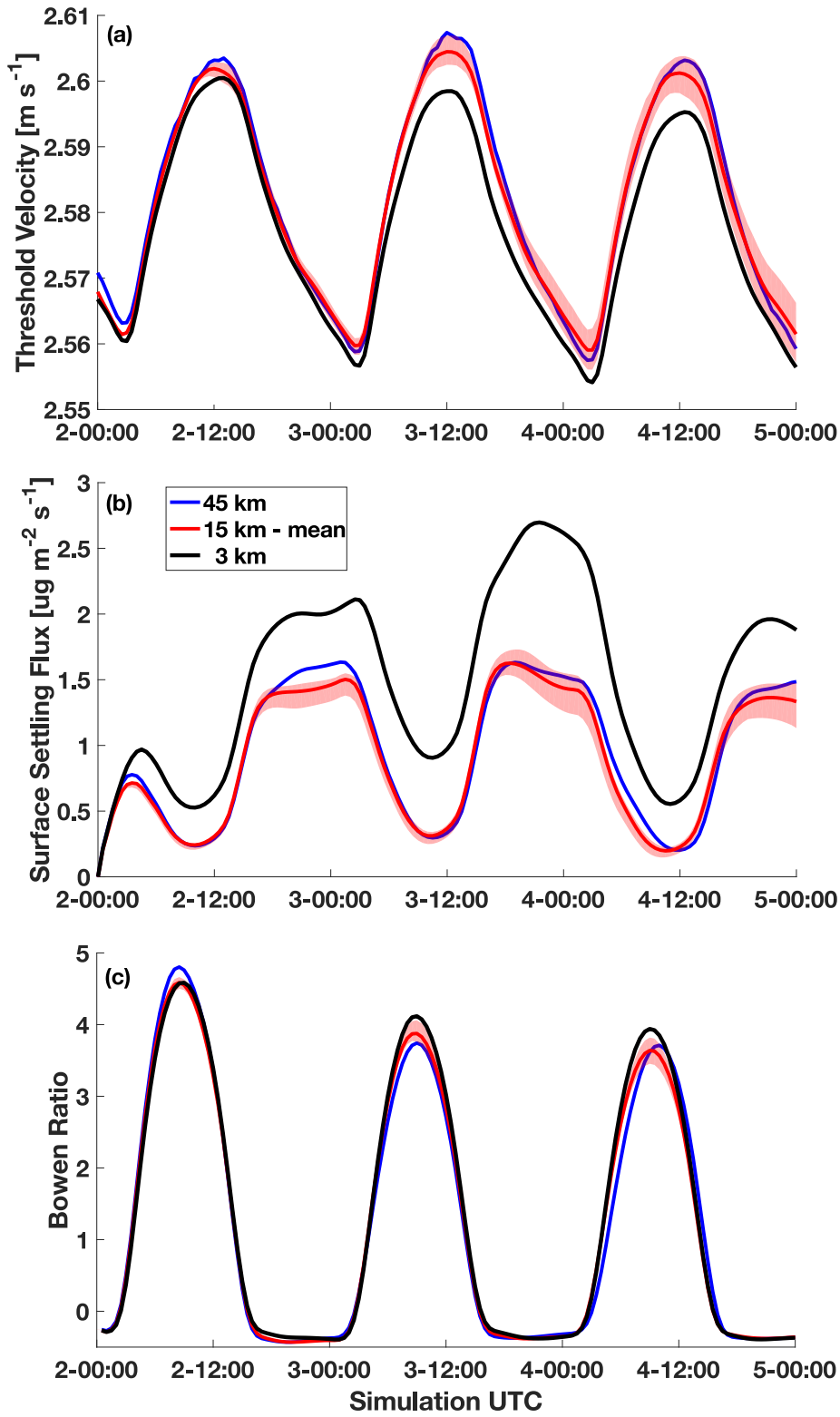
919 **Figure 5: Spatially averaged (a) dust uplift threshold velocity, (b) dust surface settling flux, and (c) Bowen ratio of**

920 **sensible to latent heat flux. Colors and shading are the same as in Fig. 4.**

921
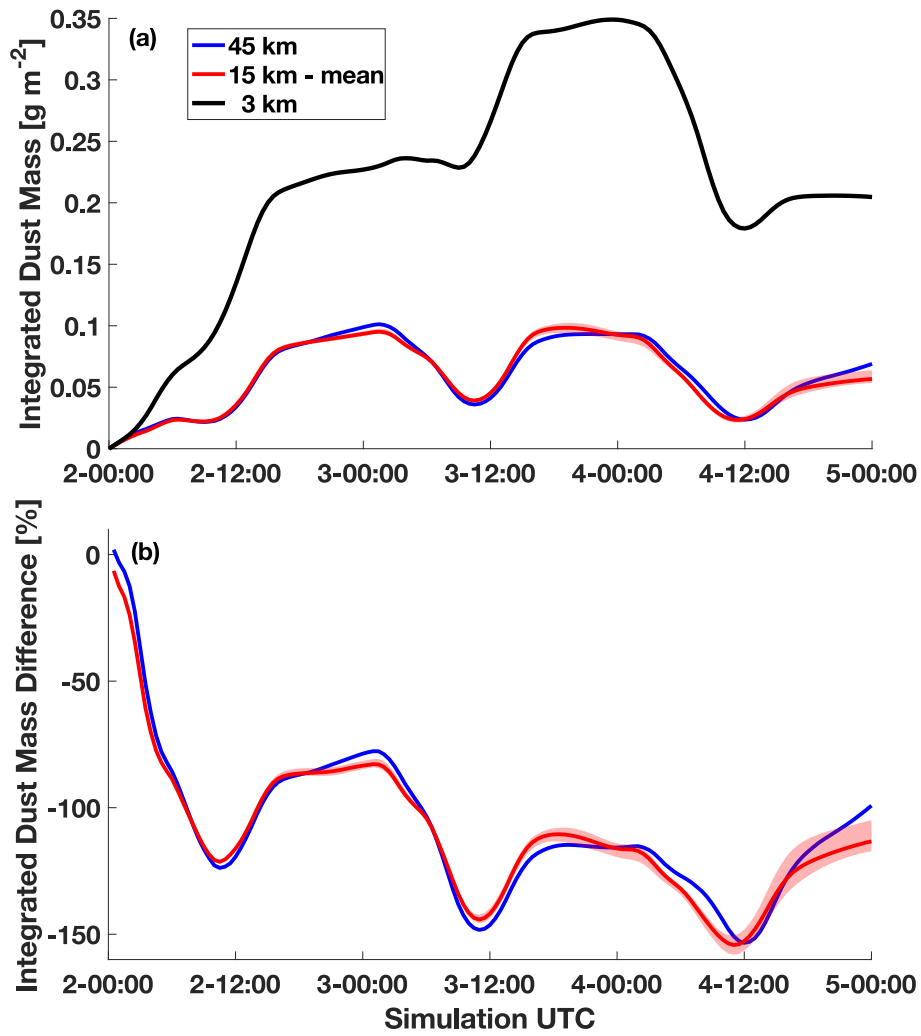
922   **Figure 6: Spatially averaged, vertically integrated dust mass. Colors and shading are identical to that in previous figures.**

923
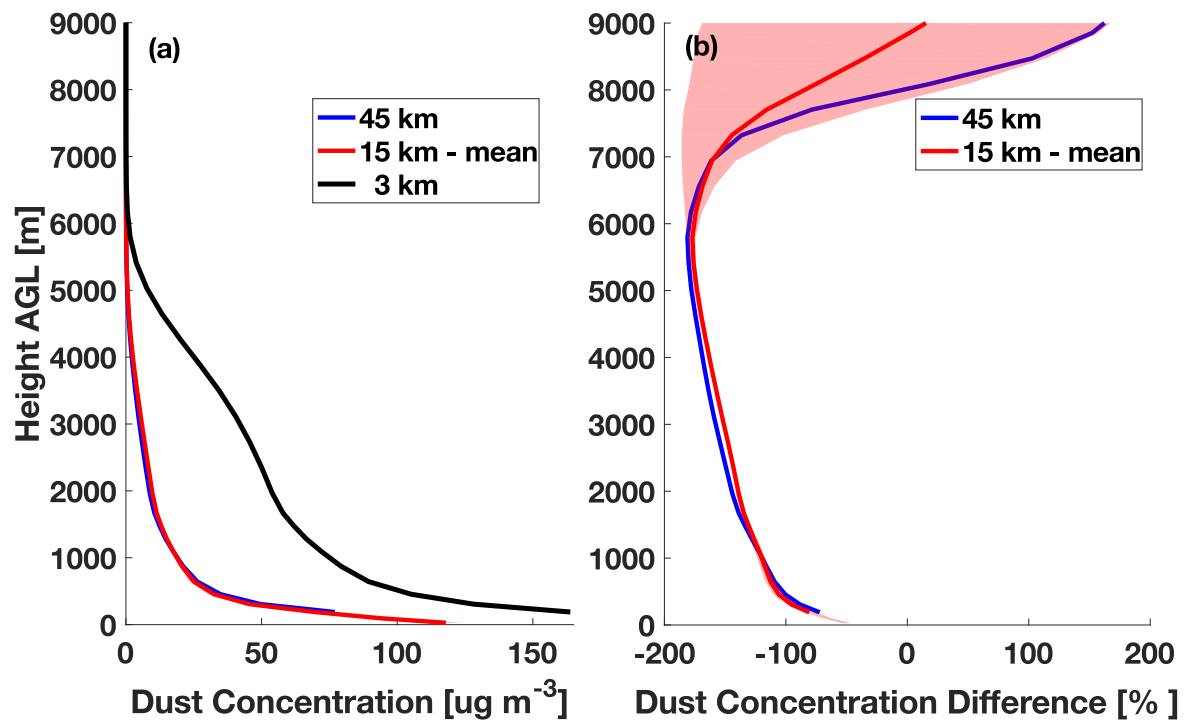
Figure 7: Spatially and time averaged vertical dust concentrations (a), with the (b) percent difference between the 3 km convection-permitting simulation and the simulations employing cumulus parameterizations. Plots are truncated at 9 km since the values above this height do not significantly vary from what is shown here. Colors and shading are identical to that in previous figures.

928
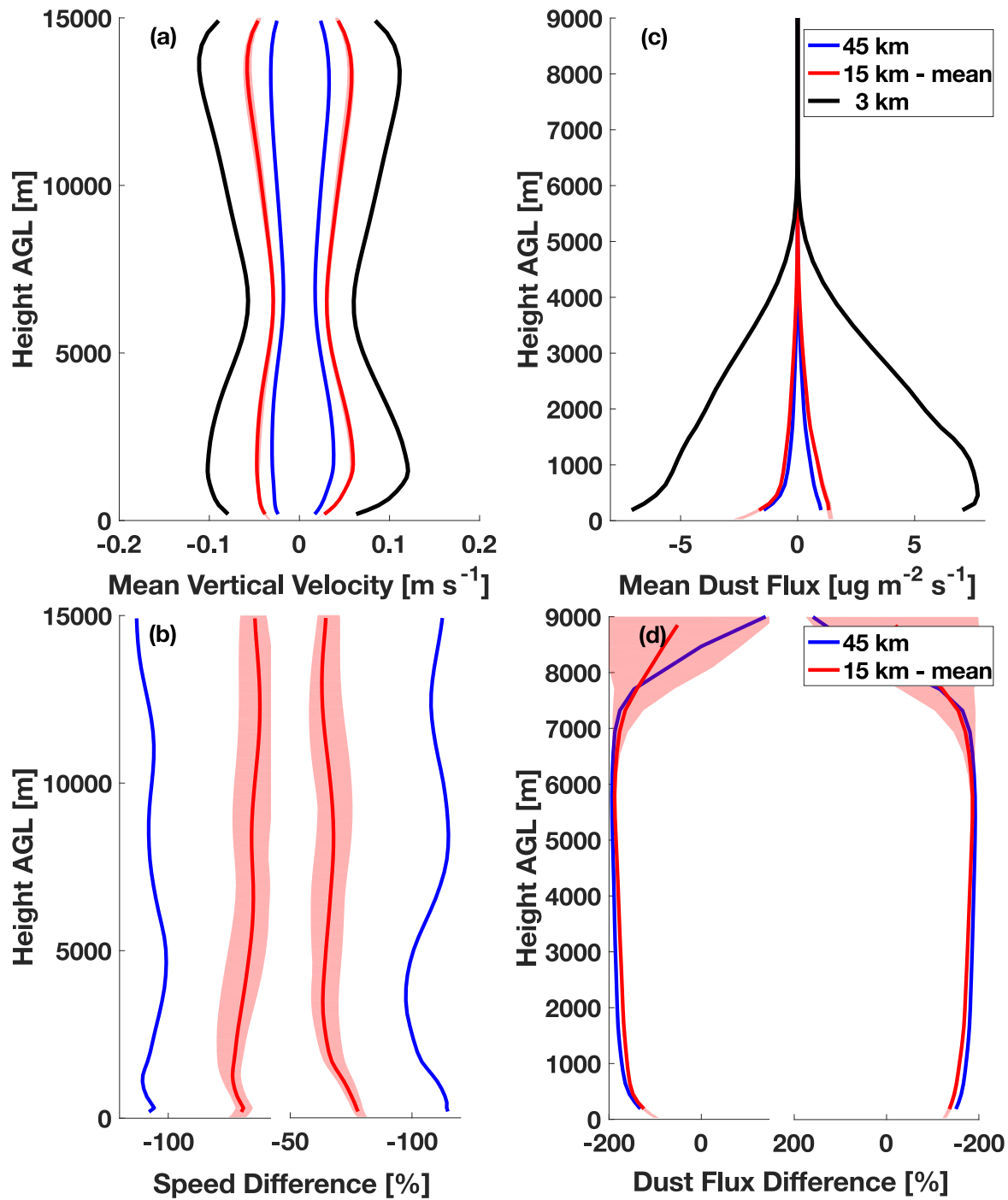
Figure 8. Left column: spatially and time averaged vertical velocities (a), with the (b) percent difference between the 3 km convection-permitting simulation and the simulations employing cumulus parameterizations. All velocities above or below zero were considered. Colors and shading are identical to that in previous figures. Right column: same but for vertical dust mass flux. Note that in panels (c) and (d) the vertical axes are truncated at 9 km since the values above this height do not significantly vary from what is shown here.
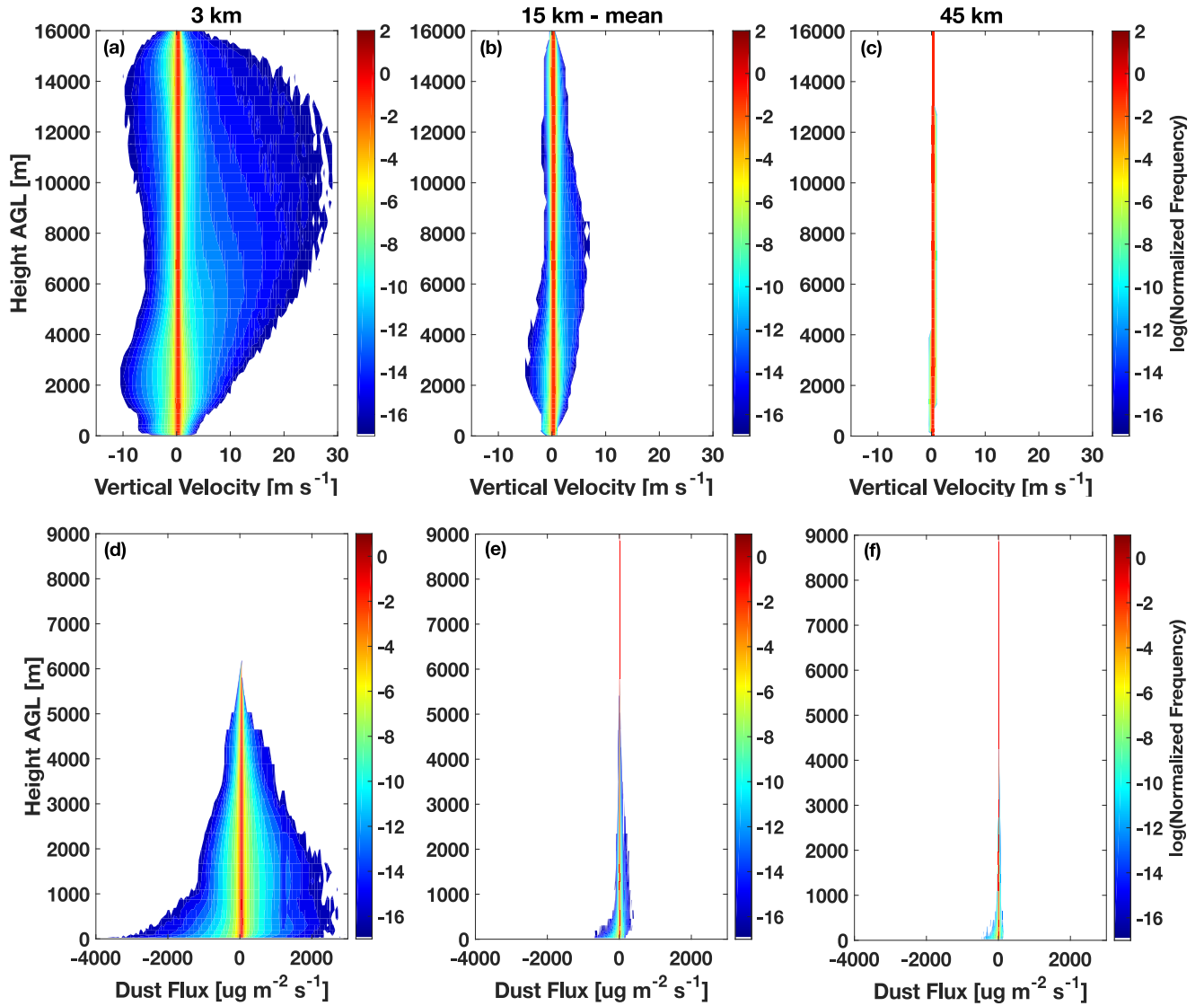
Figure 9: Top row: Contoured Frequency by Altitude Diagrams (CFADs) for vertical velocity, normalized by the number of grid points in each respective simulation. The contours are computed on a log scale to highlight the variances away from zero. Bottom row: same but for vertical dust mass flux. Note that the panels in the bottom row are truncated at 9 km since the values above this height do not significantly vary from what is shown here.

940
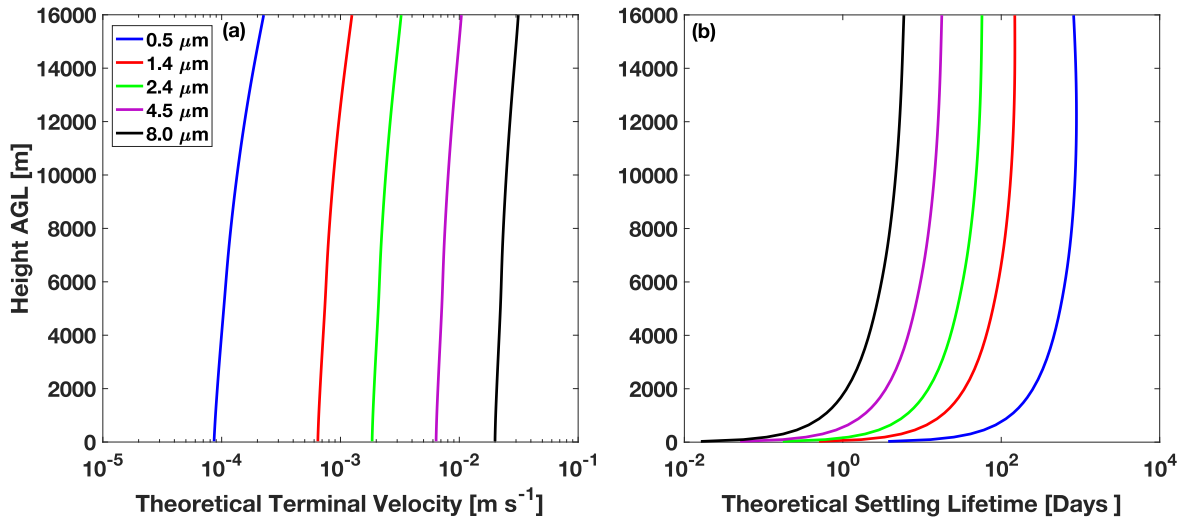
941 Figure 10: Theoretical terminal velocity of dust particles (a) based on Stokes settling velocity with slip correction for

942 pressure dependence for the 5 effective radii of dust particles in WRF-Chem. The calculations assume no vertical

943 motions, advection, deposition, coagulation, or condensation. (b) The lifetime of these theoretical dust particles based on

944 their height in the atmosphere.

945

946
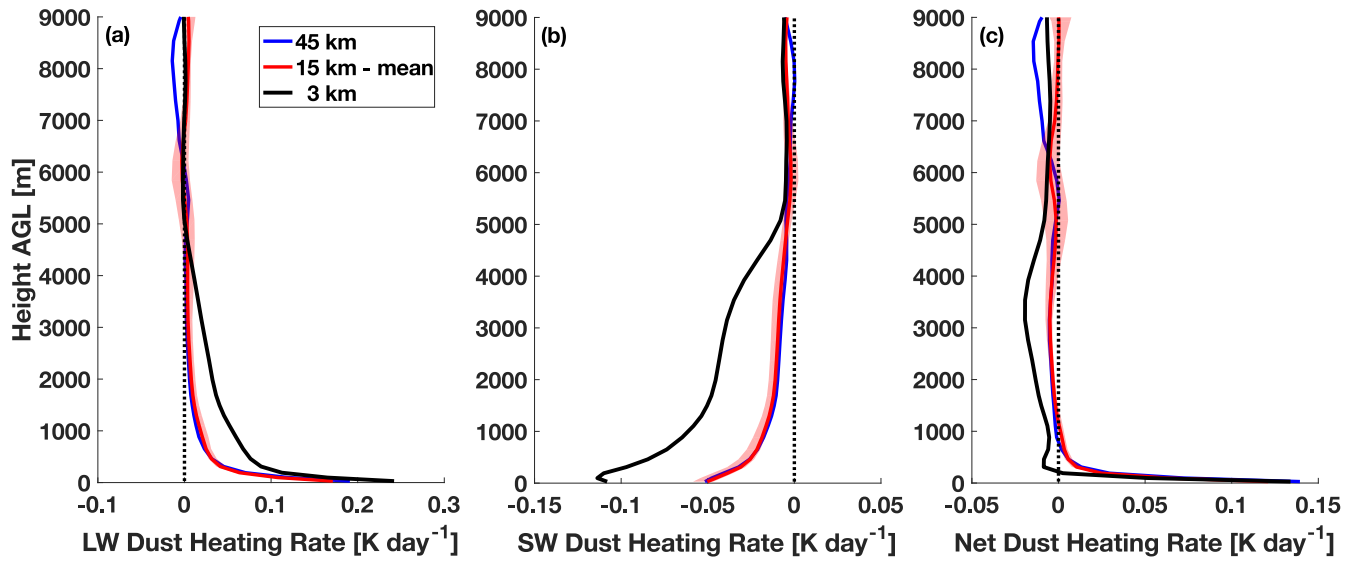
Figure 11: Spatially and time averaged longwave (a), shortwave (b), and net (c) dust heating rate profile for the 45 km
(blue), 15 km mean (red), and 3 km (black) simulations with the maximum and minimum spread across the 15 km
simulations indicated in light red shading. Plots are truncated at 9 km since the values above this height do not
significantly vary from what is shown here.